WILEY-VCH

DOI: 10.1002/ (smll.201600032)
Article type: Review

Black Phosphorus Nanosheets: Synthesis, Characterization and Applications

Varrla Eswaraiah, Qingsheng Zeng, Yi Long, and Zheng Liu**

Dr. V. Eswaraiah, Dr. Q. S. Zeng, Dr. Y. Long, Prof. Z. Liu
School of Materials Science and Engineering, Nanyang Technological University, Singapore, 639798
E-mail: LongYi@ntu.edu.sg; z.liu@ntu.edu.sg
Prof. Z. Liu
Centre for Programmable Materials, School of Materials Science and Engineering, Nanyang Technological University, Singapore,
NOVITAS, Nanoelectronics Centre of Excellence, School of Electrical and Electronic Engineering, Nanyang Technological University, Singapore 639798
CINTRA CNRS/NTU/THALES, UMI 3288, Research Techno Plaza, 50 Nanyang Drive, Border X Block, Level 6, Singapore 637553

Keywords: Black phosphorus, anisotropy, bandgap, electronics and optoelectronics.

Black phosphorus (BP) is an emerging two-dimensional (2D) material with natural bandgap which has unique anisotropy and extraordinary physical properties. Due to its puckered structure, BP exhibits strong in-plane anisotropy unlike in other layered materials. The bandgap tunability of BP enables to find a wide range of ultrafast electronics and high frequency optoelectronic applications ranging from telecommunications to thermal imaging covering the nearly entire electromagnetic spectrum whereas no other 2D material has this functionality. In this review, we discuss recent advances in synthesis, fabrication, anisotropic physical properties and BP based devices including field effect transistors (FETs) and photo-detectors. We also introduce recent passivation approaches to address the degradation of BP which is one of the main challenges to bring this material into real world applications. Finally, we comment on the recent developments in other emerging applications, future outlook and challenges ahead in BP research.

1. Introduction

Black phosphorus (BP) was discovered about 100 years ago.[1] It was noticed due to its stability compared with other phosphorus allotropes such as red, violet and white phosphorus.[1, 2] After the groundbreaking research on graphene in 2004 by Manchester scientists, this layered material opened a new branch of science and provided a vast number of unlimited applications ranging from printable electronics to prototype devices.[3-6] New physics is getting established in two-dimensional (2D) materials because the synthetic techniques are getting explored to prepare new layered materials artificially.[7-16] Black phosphorus is rediscovered due to its two dimensionality and the availability of advanced characterization techniques. BP has the great potential in field effect transistors (FETs), photo-detectors, cathode/anode material in batteries, thermoelectric applications and others owing to its unique structure, excellent physical properties and unusual anisotropy which are rarely found in other 2D materials.[17-19] Phosphorene (single layer of BP) is the second elementary single-layer material after graphene that can be exfoliated from bulk crystals, giving rise to unique functionality which can bridge the gap between graphene and transition metal dichalcogenides (TMD) nanosheets such as MoS_2, WS_2 etc., and transition metal oxides (TMOs) in terms of direct bandgap and high mobility.

BP is a semiconductor with a predicted direct fundamental bandgap of ~0.3 eV for bulk and ~2 eV for single layer,[19, 20] which is identified by high-resolution scanning tunneling spectroscopy (STS).[21] Furthermore, comparing numerous calculated and experimental results we can deduce that the optical bandgap of single layer phosphorene should be around 1.45 eV due to the huge exciton binding energy.[9, 22-24] Bandgap of BP can be largely tuned with the number of layers but always keeps direct regardless of the thickness (the direct bandgap point shifts from Γ point to Z point in the first Brillouin zone when the thickness increases from

monolayer to few-layer or bulk), which is superior to TMDs. It is of great challenge to realize tunable direct bandgap with wide range for TMD layers.[25-28] For example, thin layers of MoS_2 attracted in electronics and optoelectronics exhibit direct bandgap and high photoluminescence (PL) only with single layer,[29, 30] but the production of single layer is energy consuming and the yield is low.[31-34] Furthermore, the bandgap of BP can be tuned from semiconductor to semimetal by doping with potassium.[35] The anisotropic Dirac semimetal state was reported in this K doped BP and it allows optimization of electronic and optoelectronic devices. First-principles simulations showed that one-dimensional and even 2D Dirac cones (semimetal state) can also be produced by applying a moderate uniaxial or hydrostatic pressure on bulk or multilayer BP,[36] and this prediction of electronic topological transition was successfully realized by applying a hydrostatic pressure larger than 1.2 GPa experimentally.[37] Another interesting phenomenon by calculation is that continuous transition from the normal insulator to a topological insulator and eventually to a metal may be induced by applying perpendicular electric field on few-layer BP, and the topological band inversion originates entirely from the field-induced Stark effect.[38]

Apart from the tunability and wide range of direct bandgap in BP, a hole mobility of 300~1000 $cm^2 V^{-1} s^{-1}$ can be obtained from the FETs based on few-layer BP flakes exfoliated on Si wafer together with a large on/off ratio,[9, 18, 39] and this mobility value might be enhanced to 2000-4000 $cm^2 V^{-1} s^{-1}$ when BP flakes are located on h-BN substrate or sandwiched between two h-BN flakes at low temperature,[40-42] getting close to the hole mobility of bulk BP ~ 6500 $cm^2 V^{-1} s^{-1}$.[43] These are distinct advantages over other atomically and ultra-thin layered materials such as graphene, BN and TMDs (MoS_2, $MoTe_2$, WS_2). Therefore, it has the potential to overcome the hurdles imposed by the silicon semiconductor industry where the complexity and integrity in

designing ultra-thin membranes for channels.[44] Apart from that, BP is very sensitive to the incident light opening the doors for ultra-fast photo-detectors from ultra-violet (UV) to near infrared (NIR) region of the electromagnetic spectrum.[45-47] Also, facile top-down approach for preparation of black phosphorus quantum dots (BPQDs) in solution is presented. BPQDs mixed with polyvinyl pyrrolidone (PVP) as the active layer, a flexible memory device was successfully fabricated that exhibits a nonvolatile rewritable memory effect with a high on/off current ratio and good stability.[48]

BP distinguishes from other widely investigated 2D layered materials because of its unique crystal structure. It has a puckered structure along the armchair (AM) direction, and this structural anisotropy is due to its local bonding configurations. The bond angle along the zigzag (ZZ) direction is 94.3° and the adjacent P−P bond length is 2.253 Å. These values are smaller than the corresponding dihedral angle along the AM direction (103.3°) and the connecting bond length (2.287 Å). The lattice constants along the two perpendicular directions are different, at 3.30 Å and 4.53 Å, respectively. This kind of unique structural arrangement, resembling a network of connected hinges is the origin of the anisotropic physical properties.[49-53]

The aim of this review paper is to cover the unique anisotropic physical properties of BP for next generation electronics and optoelectronic devices. It discusses recent progress highlighting anisotropy, methods of preparing bulk BP crystals and nanosheets, and their potential applications. We also discuss passivation techniques to address BP degradation, as well as the new approaches taken to improve the device performance. Though there are a few review articles already published, we hope this review article will give some more comprehensive overview and new insight into the results due to the rapid number of publications in this area.[17, 53-58] Phosphorene and its counterpart BP received worldwide attention after its rediscovery in 2014

and continuing. It has been widely investigated from across the globe as shown in **Figure 1**a where it shows a suddenly exponential growth in the number of articles published and it has been acquired global importance (Figure 1b) for its futuristic view on technological applications.

2. Synthesis of Bulk Crystal and Thin Film/Nanosheets

BP bulk crystals are grown by several methods such as chemical vapor transport (CVT). BP thin film or nanosheets are mainly obtained via top down exfoliation process using bulk crystal. There are limited bottom up methods available currently for the growth of BP thin film while various methods have been getting explored in exfoliating BP into thin nanosheets in liquids and in solid state. A very few reports have been published on large scale exfoliation which are essential for different applications such as LEDs, printed electronics and super-capacitors. Here we describe an overview of the methods available for synthesis of bulk BP and exfoliation or growth methods for few-layer samples.

2.1. Synthesis of Black Phosphorus Crystal

Synthesis of BP can be traced back to 100 years ago and there are currently few methods available to synthesize BP single crystals such as high pressure synthesis,[1] CVT,[59] mercury catalysis[60] and liquid bismuth.[61] In 1914, Bridgman first reported that white phosphorus (WP) can be converted into BP single crystals under a hydrostatic pressure of 1.2 GPa at 200 °C within 5–30 min. It was an accidental discovery in an attempt while converting WP into red phosphorus (RP) by application of high hydrostatic pressure at moderate temperatures[1] and subsequently this method to obtain large BP crystals (**Figure 2**a & 2b) was followed by many others.[18, 62-64] Typically, in a high pressure synthesis process, RP was heated to 1,000°C followed by slow cooling down to 600°C at a cooling rate of 100 °C per hour under a constant pressure of 10 kbar and this gave a yield of high quality BP crystals with highest purity.[18] BP single crystal larger

than 5 × 5 × 10 mm^3 was achieved by melting it at a temperature of 900 °C with a hydrostatic pressure of 1 GPa as reported by Endo et al.[62] Few attempts also made to prepare BP crystals by other methods known as mercury catalysis[60] or by recrystallization of liquid Bismuth[61, 65, 66] to fabricate needle or plate type BP single crystals with 5 mm in length and 10-100 μm in thickness. However, those methods suffer from highly toxic in nature and time consuming in experimenting.

CVT method has been identified as a potential method (Figure 2c & 2d) in preparing BP crystals. Orthorhombic BP can be grown by a short way transport reaction from RP with Sn/SnI_4 as mineralization additive.[59, 67, 68] In this CVT process, there are byproducts obtained along with BP crystals such as Au_3SnP_7, AuSn, Au_2P_3 etc (Figure 2c & 2d for different portions of sample in the same ampule). To facilitate an effective and fast synthesis of BP, Köpf et al. tried to optimize the reaction conditions in such a way that the main product and unwanted phases are well separated from each other by taking excess Sn and as mineral additive.[68] Out of these methods reported in BP crystals, it is important to assess the quality of the crystal since it will have great impact on quality and doping of produced BP nanosheets, consequently influencing the properties and applications. CVT and high pressure methods offer good access to grow high quality crystals with facile fabrication though high pressure synthesis is high energetic process. Growing of BP crystals with highest purity of good yield by avoiding byproducts is still challenging and it needs further exploration.

2.2. Preparation of Thin Film and Phosphorene Nanosheets

2D materials have variety of bottom up synthesis methods such as chemical vapor deposition (CVD) using metallic catalysts,[69-73] epitaxial process,[74-76] hydrothermal methods,[77] and reduction methods,[78, 79] and even for ternary or heterostructure growth.[80-86] Unfortunately,

phosphorene is not fully explored in preparation partially due to the complicated chemistry of phosphorus. Efforts combining expertise in materials science and chemistry should be devoted to the development of large-scale synthesis methods for BP in thin film form at the wafer scale where more application opportunities emerge like other 2D materials, such as graphene.[87] It is also important to develop methods that can synthesize large-area single-crystal thin films (at least in the order of square millimeters) in which the anisotropic properties of BP may be explored at a larger scale.[88] Very recently Li et al. reported thin-film BP with the thickness of 40 nm on a flexible substrate by depositing a RP thin film on a flexible polyester substrate followed by its conversion into BP in a high pressure multi anvil cell at room temperature (Figure 2e-2g).[89] Additionally, amorphous BP film was successfully grown on Si/SiO_2 or graphene/Cu substrates via pulsed laser deposition using BP crystal as precursor,[90] producing poorly crystallized films with a thickness ranging from several nanometers to tens of nanometers. These process need to be further enhanced by optimizing the processing conditions but these approach can be advantages in synthesis of thin film in terms of processability of BP film in one step. The development of wafer-scale CVD on metal substrates[91] and epitaxial growth on insulating substrates[92] has enabled large-scale device fabrication based on graphene and TMDCs but this approach has not yet been developed for phosphorene.

High quality two dimensional nanosheets were obtained from its bulk 3D crystals by well-known top down scotch tape technique (also known as micromechanical delamination). It has been started with production of atomic layers of graphene from highly oriented pyrolytic graphite (HOPG) followed by repeatedly peeling it off. This method was used for bulk crystals such as MoS_2, ReS_2, WS_2 and other layered materials to produce the nanosheets.[3, 93-95] BP nanosheets (Figure 2h) are also prepared by same scotch tape approach from its starting BP

crystal. This is discussed in above section and they are used in BP field effect transistors.[9, 18] However, this method is not scalable since the yield is extremely low and it is challenging to test this unique material for volume applications such as energy, sensors and composites field. Liquid phase exfoliation is one of the most promising large scale techniques which is a direct conversion of bulk layered crystals into thin nanosheets stabilized by electrostatic repulsion[31, 96] in aqueous solvents and surface energy matching in organic solvent based systems.[31, 97] Hanlon et al. reported high-quality, few-layer black phosphorus nanosheets produced in large quantities by liquid phase exfoliation in the solvent N-cyclohexyl-2-pyrrolidone (CHP).[98] Metric measurement has been utilized to measure the size and thickness of BP nanosheets produced in the liquid, which are stable in CHP unless water with dissolved air is intentionally added. Sonication of ground BP crystals yields a brown dispersion, and the corresponding microscopic image depicts the typical size and dimensionality of the produced nanosheets along with high resolution TEM confirms the corrugated structure of few-layer BP flakes (Figure 2i & 2j). This means BP can be exfoliated successfully without introducing any defects like other 2D materials with this method. Up to date there are few articles published on making BP nanosheets from single to few layers in solvents such as N-methyl pyrrolidone (NMP), di-methyl sulfoxide (DMSO), and di-methyl acetamide (DMA) etc.[99-101] However, just small amounts of nanosheets can be obtained via these methods.

It is expected that phosphorene growth on metal substrates is going to be completely different with carbon crystallization and growth. Controlling number of BP layers on metal and insulating substrates is a challenging task which needs to be explored on large scale in coming years.[53] It is very important to have liquid processing approaches for few-layer BP flakes in a variety of solvents at high concentrations to be used in applications such as printable electronics, LEDs,

photo-voltaic and energy storage devices.[102] New approaches should be investigated in using mixtures of solvents to match the surface energy and maximizing the production rates of phosphorene in liquids similar to other 2D materials. High concentration and high viscous solutions of phosphorene nanosheets in variety of solvents and mixtures can be advantageous in preparing homogenous thin films and polymer nanocomposites films for multifunctional applications. Surface degradation of BP and spontaneous etching with water exposed in air limits the application of BP in aqueous based systems duo to the possible oxidation.[44, 103-105] However, one very recent report demonstrates that bulk BP crystals can be prepared by a scalable gas-phase catalytic transformation method in water and they are stable enough in water for further processing and applications.[106] Functionalization of BP can open new ways of exfoliation which can be highly stable in water. Shear exfoliation technique has been reported for making thin nanosheets of almost any 2D materials.[107-109] Woomer et al. adopted this approach to shear exfoliate BP thin nanosheets in organic liquids on large scale (10 g) using a shear mixing process by following shear exfoliation process.[110] Green liquid exfoliation of BP shows, it can be exfoliated in a range of ionic liquids reaching up to high concentrations as much as 0.95 mg ml^{-1} with high quality where it can find in-situ applications.[111]

3. Characterization of Black Phosphorus

Both BP and exfoliated thin flakes have been well characterized by different characterization techniques such as absorption spectroscopy, X-ray diffraction (XRD), neutron diffraction, scanning electron microscopy (SEM), transmission electron microscopy (TEM) and aberration corrected TEM, Raman spectroscopy, scanning tunneling microscopy (STM) and many other qualitative and quantitative techniques to understand fundamental properties of BP both in

nanoscale and bulk scale. Here we present few structural, morphological and spectroscopic analysis in this section.

3.1. Structural Analysis

BP has a layered structure consists of puckered hexagonal rings in orthorhombic crystal structure under normal conditions, while individual layers of phosphorus atoms are stacked together by van der Walls force. This structure can be reversibly transformed to semi-metallic rhombohedral phase and metallic simple cubic under ~5 GPa and ~10 GPa pressure respectively.[113] It is known that metallic simple cubic phase shows superconductivity at 6 K. **Figure 3**a shows the atomic structure of BP and each atom is bonded with three neighboring atoms. This network is formed by sp^3 hybridization. Single layer of BP is shown in Figure 3b & 3c from side and top view and it reveals the corrugated structure of each BP layer. The x and y directions corresponds to the AM and ZZ directions. It should be noted that strong in-plane anisotropy exists along these two directions. The experimental investigation on atomic structure and individual atomic appearance visually has been explored recently by Wu et al. using STEM imaging along different crystallographic directions.[114] Figure 3d shows an Annular dark field-scanning TEM (ADF-STEM) image of a BP flake exfoliated from the bulk sample viewed along the [101] direction. Here the increased spacing between atomic columns allows the individual atomic columns to be clearly visible. Figure 3e & 3f show the low- and high-magnification ADF-STEM images captured at the edge of a BP flake, which is aligned along the [100] crystallographic direction and this provides a cross-sectional view of layered 2D BP. This method of imaging can even reveal doping of any other atoms into phosphorene lattice. Bulk BP bandgap is 0.3 eV and is sensitive with number of layers in it. There have been some studies theoretically and experimentally over band gap calculations of BP and its layer dependency.[9, 19, 22-24, 115] The

density functional theory (DFT) band structures of phosphorene and calculated bandgaps with the number of layers are shown in Figure 3g & 3h. It is noted that the calculated results from GW method give a tunable bandgap from 0.3 eV to 2 eV when the thickness of BP decreases from bulk to monolayer,[19] in agree with an experimental result carried out by STS method.[21] These upper and lower bounds provide a good range of tunability in bandgap and corresponding electronic properties.

3.2. Spectroscopic Analysis of BP

BP is characterized by various spectroscopic techniques such as Raman spectroscopy, Infrared spectroscopy, Photo-luminescence (PL) spectroscopy, and polarization dependent spectroscopy and X-ray photoelectron spectroscopy. These techniques can find the characteristic vibrational modes, intrinsic bonding energies, crystallinity and crystallographic directions. Spectroscopic techniques also been used to study the vibrational properties of thin BP nanosheets by external stimuli such as strain, temperature and pressure to unravel the intrinsic anisotropic physical properties which are arising due to unique puckered structure of BP. Raman spectral features are sensitive to the number of layers in BP, such as the intensity ratio of A_{2g} to A_{1g} modes showing a monotonic discrete increase with the decrease of thickness down to a monolayer.[116] It is depicted that Raman analysis can be indirect way of finding number of layers in flakes but with careful experimentation, for example choice of substrate and crystalline orientation to the polarization of incident laser, however the accuracy of number of layers depends on resolution of spectrometer. The typical spectra of bulk BP consists of main features at 362 cm^{-1}, 439 cm^{-1}, 467 cm^{-1} which are attributed to A_g^1, B_{2g} and A_g^2 phonon modes respectively[117] from the examined flake (**Figure 4**a & 4b). The B_{2g} and A_g^2 modes correspond to vibrational modes where the

atoms oscillate within the phosphorene layer plane, in the A_g^1 mode the phosphorus atoms vibrate out-of-plane. Xia et al. studied polarization resolved Raman spectroscopy in order to address the anisotropic behavior and layer dependency in different crystalline orientations.[112] The Raman scattering results for laser excitation along x, y and D (diagonal) directions indicates that (Figure 4b) the standard peaks of BP which appear in all directions displays regardless of the polarization. For all three different polarization, it appears that there is no change in the position of Raman peaks but there is relative change in the intensities of A_g^1, B_{2g} and A_g^2 phonon modes of characteristic peaks which changes significantly with polarization direction. For example, B_{2g} mode peak intensity changes along D direction abruptly because the intensity of this mode is determined by the off diagonal polarizability tensor α_{xy} which is maximized at 45° orientation. The intensity changes in both A_g^1 modes accompanied by the diagonal and off-diagonal polarizability tensor and the reasons need to be explained in future. This polarization dependency continues up to thickness of 3 nm BP films and this can be used to find the crystalline orientation of BP crystals by a spectroscopic technique. Detailed comprehensive studies have been performed on finding crystallographic directions of BP (AM or ZZ) using angle resolved polarized Raman spectroscopy.[118, 119] These studies discovered that Raman modes of BP not only depends on the polarization angle (the angle between the polarization vectors of incident laser and scattered light) but also rely on sample rotation angle (the angle between the AM direction of BP and polarization vector of scattered light). The polarization dependency of Raman modes in BP is extensively investigated by exciting it with different wavelengths.[120] According to their report, B_{2g} doesn't show polarization dependence irrespective of thickness and change in excitation wavelengths whereas A_g^1 and A_g^2 exhibits

peculiar dependency. The thickness dependency can be due to birefringence and dichroism of the BP whereas wavelength dependency is explained on fail-proof concept.[120] Low frequency shear Raman modes in layered materials are very sensitive to the number of layers which is proved in graphene[121] and MoS_2.[122] Similarly low frequency Raman modes are theoretically and experimentally investigated in BP as well to probe intercoupling interactions and crystallographic orientations,[123-126] and the results show that these anisotropic modes are much more sensitive to the layer number (than those in other 2D materials and the high frequency mode of BP) due to the several times larger interlayer forces existing in BP layers, which may originate from stronger overlapping of interlayer orbit caused by more significant charge redistributions.[125] Raman spectroscopy also can be used to estimate the thickness of the flake by calibrating the intensity of A_g^1 mode with respective silicon intensity (Figure 4c).[117]

Mechanical strain is an effective external stimulus on phosphorene which can be studied in depth by Raman spectroscopy and it will also modulate the electronic band structure. Theoretical studies from Fei et al. show that strain conditions can be monitored from the shift in the position of original strain-free Raman peaks to strained phosphorene as well as the relative frequency shifts between the different peaks (Figure 4d).[127] According to their studies, the vibrational modes of monolayer phosphorene and their characteristic peaks exhibits substantial shifts according to the type and amount of applied strain. Both B_{2g} and A_g^2 modes exhibit monotonic shifts which are red-shifted when stretched and blue shifted when compressed along zig-zag direction whereas the magnitude of frequency shifts along arm-chair direction is much smaller than in the case of zig-zag strain. This is because phosphorene is rippled along the AM direction and it is softer along zig-zag direction,[127] in other words, the primary change reduced by strain is the reductions in the bond angles rather than the bond lengths.[126] Likewise, temperature also

can give substantial shifts in Raman spectra of BP.[128, 129] It is characterized by a linear equation $\omega = \omega_0 + \chi T$, where ω_0 is mode frequency at zero K and χ is the first-order temperature coefficient. The reported χ values for different modes within a low temperatures range from 20°C to -160° C can be seen in Figure 4e. The reported χ values for modes A_g^1, B_{2g}, and A_g^2 in the 5L sample are -0.023, -0.018, and -0.023 cm^{-1} $°C^{-1}$, respectively. It is noteworthy to mention, these coefficient values are larger than for graphene, MoS2, $MoSe_2$ and WSe_2[130-132] but less than that of TiS_3 nanosheets.[133] Therefore, BP is very sensitive to the applied temperature which is arising due to its corrugated structure and good mechanical flexibility. The change in frequency can be ascribed to anharmonic terms in the lattice potential energy related to pure temperature effect, and the thermal expansion of the crystal.[123] Later, Raman spectra was recorded for few layer BP in high temperature, 77 K to 673 K[129] and the softening of Raman modes is attributed to double resonance process.

Spatial inhomogeneity is of particular interest in phosphorene due to its puckered structure and strain can modify wide range of properties such as electrical and mechanical properties. Confocal Raman or near field Raman scattering can provide higher resolutions in spatial strain distribution. Zhang and co-workers investigate PL spectra of few-layer BP exfoliated on silicon substrate,[134] obtaining a high layer number dependent results (2 layers to 5 layers). Strong PL peaks are noticed at 961 nm, 1268 nm, 1413 nm and 1558 nm in 2, 3, 4 and 5-layered flakes, which are corresponding to energy peaks of 1.29 eV, 0.98 eV, 0.88 eV and 0.80 eV, respectively (Figure 4f). The PL peaks were attributed to the nature of excitons, which represent lower bounds on the fundamental band gap values in few-layer BP. The energy position of the measured PL peak increases rapidly as the layer number decreases. This indirectly confirms the theoretical calculation results that the band gap of few-layer BP increases rapidly as the layer

number decreases, which might originate from the smaller band dispersions of valence band (VB) and conduction band (CB) for thinner BP due to the weaker interlayer interaction.[23]

4. Anisotropic Characteristics

Black phosphorus has specific advantages over graphene and transition metal dichalcoginides for electronics and optoelectronics. It has unique in plane anisotropic physical properties unlike most of other 2D materials. Anisotropy of any physical property refers to the change of that property in different directions. Though it is not new in materials but quit exciting in new 2D material BP due to its large magnitude in anisotropy comparing with other 2D materials. In-plane anisotropy can open pathways for designing novel electronic and optoelectronic devices. Here we attempted to highlight the anisotropy of BP in electrical, thermal, vibrational, mechanical and spectroscopic properties by experimental and theoretical approaches.

4.1 Anisotropy of electronic structure.

Due to its orthorhombic puckered structure of BP, the effective mass of carriers shows 10 times more in ZZ direction than that in AM direction.[88] Fei et al. predict that the effective mass of electrons is highly anisotropic and appears approximately “8” shape in real space for intrinsic monolayer phosphorene,[49] as shown in **Figure 5**a. These values can differ by one order of magnitude along different directions. Such anisotropic effective mass or band dispersion is responsible for the observed anisotropic electric conductance in phosphorene.[9] This spatial anisotropy of electron effective mass can be rotated by 90° while keeping the approximate “8” shape by applying appropriate uniaxial or biaxial strain (e.g. 5% biaxial strain). Now the electrons have a very small effective mass along the ZZ direction and a large effective mass along the AM direction (see Figure 5b). It is noted that the anisotropy of holes is not perturbed at

all during this strain process and this phenomena results from a switch in the energy order of the lowest two conduction bands. Angle resolved DC conductance was measured by Liu et al. and Xia et al.[9, 112] 12 electrodes were placed on the same BP flake spaced at an angle of 30° as shown in Figure 5c. The measured DC conductance was plotted in polar coordinates from each pair of opposite electrodes separated by 180°. The resulting conductance data nicely fits into low field conductivity in an anisotropic material and provide $\frac{\sigma_x}{\sigma_y} = 1.5$.

4.2 Anisotropy of photonic and excitonic structure.

Phosphorene exhibits strong anisotropy when it is excited by polarized laser on AM-ZZ (x-y) plane.[24] Figure 5d indicates the Intensity of the $A_g^{\ 2}$ mode as a function of the excitation laser polarization angle in the x–y plane.[127] Strongest intensity of $A_g^{\ 2}$ mode is confirmed when the laser polarization is parallel to the AM direction. This method has been widely adopted to confirm the crystalline orientation of the BP crystal. This intensity of $A_g^{\ 2}$ mode fits well to a $\cos^2\theta$ function (where θ is the angle between the x axis and the polarization of the excitation laser) plus an offset, as shown in Figure 5d. The highest photoluminescence intensity occurs when both excitation and detection polarizations are aligned with the x direction.[24] The emission intensity along the y direction is consistently less than 3% of that along the x direction, regardless of the excitation light polarization (Figure 5e). First-principles simulations indicate that the anisotropic optical responses are dominated by the unique anisotropic atomic structure of BP, and the dipole selection rules determine whether a transition is allowed or forbidden based on the symmetry of the valence and conduction wave functions.[19, 135]

4.3 Anisotropy of mechanic structure.

The mechanical properties of black phosphorus nanosheets exhibit strong anisotropy in Young's modulus. First-principles calculations suggested that BP showed a strong anisotropic Young's modulus along different orientation of the BP crystals. Recent results on single layer BP suggests that there is a third principal direction in which young's modulus is maximum other than zig-zag and AM directions.[136] However, experiments are still needed to confirm this concept. The Poisson ratio also shows highly anisotropic (Figure 5f). Theoretical investigation of negative Poisson's ratio of single-layer BP was also carried out using first-principles calculations.[52] This intrinsic behavior would be observed in the out-of-plane direction under uniaxial deformation in the direction parallel to the pucker of BP. Strong anisotropic elastic modulus was calculated by Qiao et al and the results show that the values along ZZ direction are several times larger than AM direction for few-layer BP.[23] Similarly, Interlayer force constant of the ZZ direction is also more than three times that of AM due to the highly directional nature of the lone pair.[126] Wang et al. laid the framework for describing the mechanical resonant responses in free-standing BP structures using a combination of analytical modeling and numerical simulation.[137] In rectangular BP resonators, strong anisotropy in resonant frequency as shown in Figure 5g. It summarizes the mode shapes and f_{res} values for the first six resonance modes as functions of θ, the relative orientation between the crystalline stiff axis and the rectangular long side, varies between 0° and 180°.

4.4 Anisotropy of thermal properties.

In-plane anisotropy in thermal conductivity of BP is striking since no other 2D materials have shown similar performance.[138] First principal calculations over BP suggested that there is good range of anisotropy in thermal conductivity along ZZ and AM directions. For example, Fei et al. firstly theoretically discussed the anisotropic thermal conductivity of phosphorene and pointed

out that the prominent electrical and thermal conducting directions were orthogonal to each another, which indicated that the best thermoelectric performance can be obtained in the AM direction.[139] Jain et al. predicted thermal conductivity of 110 $Wm^{-1}K^{-1}$ along zig-zag and 36 $Wm^{-1}K^{-1}$ along AM directions at a temperature of 300 K.[140] Qin et al. reported the intrinsic lattice thermal conductivity of phosphorene by solving the phonon Boltzmann transport equation based on first-principles calculations.[141] Their results show that thermal conductivity of phosphorene at 300 K is 30.15 $Wm^{-1}K^{-1}$ along ZZ direction and 13.65 $Wm^{-1}K^{-1}$ along AM direction, showing an obvious anisotropy along different directions. The reason behind anisotropy may be due to anharmonic effect, anisotropic Grüneisen parameter, and anisotropic phonon dispersion leading to direction dependent group velocities. Thermal conductivity of BP decreases with increase in temperature as expected for a phonon dominated crystalline material.[139-141] The calculated thermal conductivity fits perfectly to the inverse relationship with temperature when the temperature is higher than Debye temperature (ΘD = 278.66 K).[141] In comparison to graphene, the minor contribution around 5% of the ZA mode is responsible for the low thermal conductivity of phosphorene. Furthermore, this in-plane anisotropy can be tuned by applying external strain over the BP. Ong et al. reported anisotropic thermal conductivity as a function of external strain applied over black phosphorus using first principal calculations.[142] When the strain is applied in the AM direction, thermal conductance in ZZ direction (G_{ZZ}) decreases along with the thermal conductance in AM direction (G_{AM}). However, when the tensile strain is applied in the ZZ direction, G_{ZZ} actually increases by a small but perceptible amount. This anomaly in the change in G_{ZZ} and G_{AM} implies that the thermal conductance anisotropy can be modulated by changing the direction of the applied strain.

In-plane anisotropic thermal conductivity in BP flake was investigated using micro Raman spectroscopy by exciting with 632.8 nm wavelength laser.[143] It was found that thick BP films (>15 nm) showed anisotropic ratio of 2 whereas thin BP films (<9.5 nm) exhibited 1.5 (Figure 5h). Anisotropic thermal conductivity measurements were also carried out by Lee et al.[144] but on BP nanoribbons and measured at different temperatures above 100 K with steady state longitudinal heat flow. They discovered that, thermal conductivity decreases with decrease in BP nanoribbon thickness and anisotropy ratio stays constant (~2) within this range (~300 nm to ~50 nm). It was also concluded that ZZ nanoribbons has higher thermal conductivity than AC nanoribbons above 100 K but similar value in the temperature range of 30 to 100 K and maximum anisotropic ratio (~2) was obtained at 300 K (Figure 5i). Room temperature thermal conductivity of the exfoliated BP was measured for three crystalline axes by time domain thermos-reflectance.[145] The measured thermal conductivity along zig-zag direction was ~86 $Wm^{-1}K^{-1}$ whereas along AM direction was ~34 $Wm^{-1}K^{-1}$, which is 2.5 times lower than that of ZZ direction. Time resolved magneto optical Kerr effect was also used to estimate the anisotropy in thermal conductivity of BP flake and measured it along three principal axes of BP.[146] According to them, the measured thermal conductivity through plane is ~20 times smaller than ZZ direction and anisotropic ratio of ~3 was recorded at room temperature. The small deviations in anisotropic ratio with different experimental techniques can be due to BP morphology and measurement methods.

5. Transport Behaviors and Photodetector

The transport properties of black phosphorus fall between graphene and TMD materials. As illustrated in table 1, the mobility of the BP flakes is higher than transition metal chalcogenides and the on/off ratio is much larger than graphene, which is fundamentally and technologically

important to have higher mobility than silicon based and organic electronics. There has been tremendous amount of work done both theoretically and experimentally to know and optimize the efficient transport behavior in single layer and few layer BP primarily in field effect transistors and photodetectors.[58]

5.1. Field Effect Transistor

One of the best applications of BP is in FETs and these are generally characterized by two parameters which are mobility and on/off ratio. The very first report on BP layered material for field effect transistor reported simultaneously by Liu et al and Li et al. in 2014.[9, 18] It has become widespread research due to its ambipolar FET.[39, 147-149] The drain current modulation (10^5) at room temperature is four orders of magnitude larger than that in graphene and the large hole mobility (~1000 $cm^2\ V^{-1}\ s^{-1}$) is superior to that of commercial silicon-based devices,[58] as shown in **Figure 6**a. BP is highly anisotropic layered material in 2D family in terms of Hall mobility and electronic properties along ZZ and AM directions. Xia et al. measured Hall mobility of BP for thickness of 8 and 15 nm along x and y directions after identifying the crystalline directions (Figure 6b).[112] The hole mobility along the x direction exceeds $600\ cm^2\ V^{-1}\ s^{-1}$ at room temperature and is above $1{,}000\ cm^2\ V^{-1}\ s^{-1}$ at 120 K for 15 nm thick sample whereas for the 8 nm sample, the mobility along the x direction exceeds $400\ cm^2\ V^{-1}\ s^{-1}$ at room temperature and is above $600\ cm^2\ V^{-1}\ s^{-1}$ at 120 K. For both thicknesses, the Hall mobility along the x direction is about 1.8 times large compared with that in the y direction, indicating an anisotropy. Similar field-effect mobilities were also reported by various groups.[9, 18, 39, 150] Although most of BP FETs behave p type or ambipolar, unipolar n type FET was also realized based on aluminium-contacted 3 nm BP flakes (Figure 6c) by Perello et al.,[151] resulting in a switching with on/off ratios greater than 10^5 (10^7) and electron mobility of 275 (630) cm^2V^{-1}

s^{-1} at 300 K (80 K). Aluminium works as a good n-type contact for BP flakes because the work function of Al (4.0-4.3 eV) well align with the CB of BP, which has a minimum about 4.1 eV for 3-5 layer samples and weakly depends on flake thickness.[22] In bulk BP crystals, hole mobility values above 1,100 and 5,000 $cm^2 V^{-1} s^{-1}$ along the x direction were previously reported at 300 and 30 K, respectively.[43] As a result, future improvement in BP thin film material quality is likely to result in much enhanced mobility.

BP is a promising candidate for the application of future high frequency electronics due to the good current saturation properties arising from the finite band gap, resulting in a better performance than graphene in term of voltage and power gain. Wang et al. demonstrated the operation of BP FETs at gigahertz frequency for the first time (Figure 6d & 6e).[152] The standard ground–signal–ground (GSG) pads were fabricated and the result shows that the short-circuit current-gain cutoff frequency f_T is 12 GHz and the maximum oscillation frequency f_{max} is 20 GHz in 300-nm channel length devices (Figure 6e). Two-dimensional electron gases (2DEG) were created in black phosphorus placed on a hexagonal boron nitride (*h*-BN) substrate using a gate electric field recently.[40] The Shubnikov–de Haas (SdH) quantum oscillations in the magneto-resistance R_{xx} was observed in BP for the first time due to the high carrier mobility. The gate voltage and magnetic field dependence of these oscillations for holes and electrons at T = 0.3 K are shown in Figure 6f and Figure 6g respectively, and angle dependent oscillation was also investigated due to the anisotropy of BP, paying the way to get crucial information about the system such as cyclotron mass and lifetime of charge carriers. Stable sandwiched heterostructures by encapsulating thin BP between h-BN layers were also designed to realize ultra-clean interfaces.[41, 42, 153] Mobility as high as several thousand $cm^2 V^{-1} s^{-1}$ can be reached at low temperature for both hole and electron in this structure, and quantum Hall effects and SdH

oscillations were observed at relatively low magnetic field. Avsar et al. fabricated fully encapsulated ultrathin BP FETs under inert gas conditions by utilizing graphene as source/drain electrodes and *h*-BN as an encapsulation layer and also top gate dielectric,[154] as shown in Figure 6h. The linear I_{SD}-V_{SD} behavior shows that graphene electrodes lead to barrier free contacts, and such one atom-thick conformal source/drain electrodes also enable the black phosphorus surface to be sealed by *h*-BN layer to avoid rapid degradation. CMOS inverter consisting of BP PMOS and MoS_2 NMOS transistors (Figure 6i)[9, 155] and BP/MoS_2 van der Waals heterojunction p-n diode[156] were fabricated, providing possibilities for exploiting 2D materials based integrate circuits.

Additionally, BP is also potential to be used in flexible and wearable electronics due to its 2D properties. Zhu et al. reported flexible ambipolar transistors, circuits and amplitude-modulated demodulator using black phosphorus.[157] Few-layer BP was placed on a flexible polyamide (PI) substrate with Al_2O_3 encapsulation and cured polyimide was coated on both sides to maintain the stability. Transfer characteristics of encapsulated BP FET (Figure 6j) exhibits negligible hysteresis due to effective encapsulation and protection against moisture absorption. The extracted low-field hole mobility was 310 $cm^2\ V^{-1}\ s^{-1}$, which is much higher than state-of-the-art semiconducting TMD, organic and metal oxide flexible transistors.

5.2. Photodetectors

Optoelectronic devices are electronic devices that can generate, detect, interact with or control the light. Variety of nanomaterials such as carbon nanotubes, semiconductor quantum dots and nanowires have been much studied for use in optoelectronic applications such as lasers, LEDs, solar cells, optical switches, photodetectors and displays.[158-166] The main challenge in bringing 2D nano-sheets for photo-detectors is to get the high responsivity along with ultrafast response

covering broad ranges of detection in electromagnetic spectrum. The absence of natural bandgap in graphene reduces its applicability in photodetectors. 2D semiconductors, TMDs and some other 2D materials show interesting optoelectronic properties but they have higher bandgap which are useful only some part of the visible electromagnetic radiation.[167-171] Therefore, there is a high demand for ultrafast photodetectors using 2D nanosheets with small bandgap to cover the main portion of electromagnetic spectrum.[172, 173] BP has intrinsic and tunable direct bandgap which satisfies the requirement to fulfil the above criteria, which was proved by a few reports about bulk BP crystal.[63, 174] Layered phosphorene has remarkable in-plane properties and it exhibits strong anisotropy in optoelectronic properties when illuminated by electromagnetic (EM) radiation. Highly anisotropic photonic properties of BP have been discussed above. It needs to be investigated in much more details on how anisotropic photo-response can be used in practical applications. There are many possible exciton dynamics and mechanism of photo-current generation in BP devices such as photoconductive,[46, 175] photovoltaic,[176] photo-thermoelectric and bolometric effect[177] since these phenomena are influenced by operating and experimental conditions. In this section, we attempted to give a comprehensive overview and analysis of the published results of BP photodetectors and compare the performances with other 2D nano-sheets for the optoelectronic applications.

Buscema et al. investigated the photoresponse of FETs based on 3−8 nm thick BP flakes from the visible region up to 940 nm, as shown in **Figure 7**a.[175] The responsivity of 4.8 mA W^{-1} and a rise time of about 1 ms were realized for 640 nm laser illumination. The cutoff wavelength (λ_{cutoff}) to be around 997 nm (1.24 eV) from the linear fit data, which is larger than previously reported photodetectors based on 2D materials such as MoS_2,[167, 178, 179] WS_2,[180] GaSe[181] and GaS,[182] indicating that BP can be used as active material for broadband photo detection.[175] Wu

et al. showed that experimentally BP (thickness 4.5 nm) also can be used as sensitive photo-detector in ultraviolet range for the first time (Figure 7b),[46] demonstrating a specific detectivity ~3 ×10^{13} Jones and an enhanced responsivity up to ~9×10^{4} A W^{-1} at 3 V bias, which is the highest value reported for black phosphorus. The colossal responsivity can be attributed to the resonant-interband transition between two specially nested valence and conduction bands with an unusually high density of states for highly efficient UV absorption. Apart from above mentioned photoconductive devices, photovoltaic device was also fabricated based on few-layer BP flakes with split gates and hexagonal boron nitride dielectric.[176] Local charge carrier type and density were controlled by electrostatic doping in the device. Zero-bias photocurrents and significant open-circuit voltages were observed in such illuminated gate-defined PN junction due to the photovoltaic effect (Figure 7c) in the visible and near-infrared range. Deng et al. studied the photodetection performances of a gate-tunable p−n diode based on a p-type black phosphorus/n-type monolayer MoS_2 van der Waals p−n heterojunction,[156] realizing a maximum photodetection responsivity of 418 mA W^{-1} at the wavelength of 633 nm and photovoltaic energy conversion with an external quantum efficiency of 0.3%. Engel et al. fabricated BP photodetector on Si/SiO_2 substrates (BP thickness is 120 nm) to record diffraction-limited images of microscopic patterns in the visible and near-infrared spectral regime.[45] Their BP device is capable of acquiring high-contrast ($V > 0.9$) images both in the visible (λ_{VIS} = 532 nm) as well as in the infrared (λ_{IR} = 1550 nm) spectral regime. Experimental resolution of 270 nm and 720 nm were achieved with 532 nm and 1550 nm wavelength respectively, and that fits well into width of model point spread function which is used to estimate theoretical resolution limit. The same BP photodetector has been investigated imaging capabilities for complex structures, and the

integration time per pixel in the image is 10 ms, which results in a total image acquisition time of 12 min, a typical value for practical confocal microscopy.

Qiao el al. predicted the optical linear dichroism behavior of BP between perpendicular in-plane directions,[23] allowing the determination of the crystalline orientation and optical activation of the anisotropic transport properties. Polarized photoresponse of BP was investigated by several groups.[46, 183, 184] Yuan et al. reported polarization sensitive broadband photodetector using a black phosphorus vertical p–n junction device over a bandwidth of 400 to 3750 nm.[184] A ring-shaped metal electrode was designed as an isotropic photocurrent collector to exclude the influence from the orientation of the electrode edge, as shown in Figure 7d. The polarization sensitivity is due to the strong intrinsic linear dichroism, which arises from the in-plane optical anisotropy of this material. A perpendicular built-in electric field in this transistor geometry induced by gating can spatially separate the photo generated electrons and holes in the channel, effectively reducing their recombination rate and thus enhancing the performance for linear dichroism photodetection. Photocurrent microscopy images of the BP have been recorded inside the inner ring under illumination at 1,500 nm with different light polarizations (along x direction is shown in Figure 7e), and the photoresponsivity to polarized laser excitation with wavelength varying from 400 nm to 1,700 nm indicates the wide bandwidth of the linear dichroism detection (Figure 7f).

BP also shows feasibility of applications in high speed optical communication. Youngblood et al. demonstrated a gated multilayer black phosphorus photodetector integrated on a silicon photonic waveguide with few-layer graphene as top-gate operating in the near-infrared telecom band.[47] In a significant advantage over graphene devices, black phosphorus photodetectors can operate under bias with very low dark current and attain an intrinsic responsivity up to 135 mA

W^{-1} and 657 mA W^{-1} in 11.5 nm and 100 nm thick devices, respectively, at room temperature. The photocurrent is dominated by the photovoltaic effect with a high response bandwidth exceeding 3 GHz at low doping regime, while it is dominated by bolometric effect with a much lower cut-off frequency (~0.2 MHz) at highly n-doping regime, as shown in Figure 7g. The measured completely open eye indicated that the BP photodetector can be readily used for practical optical communication. Recently, terahertz frequency photo-detector was constructed experimentally with 10 nm thick BP flake as an active channel in FET.[185] The source and gate electrodes were patterned in the shape of two halves of a planar bow-tie antenna with a total length of 500 μm and a flare angle of 90° (Figure 7h), in resonance with the 0.3 THz radiation. The mobility of 470 cm^2 V^{-1} s^{-1} was obtained and a maximum responsivity of 0.15 V W^{-1} was reached for this top-gated FET. Major improvements can be envisioned by engineering wide gate architectures and impedance matched nano-antennas to address targeted terahertz application requirements.

Polarization-sensitive photodetection of BP provides new functionalities in novel optical and optoelectronic device applications. A possible method for enhancing the electronic and optoelectronic performances of BP devices is selecting the metal contact to tune the Schottky barrier height between contact and semiconductor channel, and there are already some experimental attempts,[186, 187] and as well some theoretical simulations.[188] More recently, Ni/Au contacted BP short channel FETs show an ultrahigh photoresponsivity up to 10^6 A W^{-1} within a wide wavelength range from 400 nm to 900 nm at room temperature.[189] In order to compare the photodetection performances of BP with other 2D materials, we list responsivity and photoresponse time of various 2D materials in different regimes of electromagnetic spectrum in Table 2.

6. Instability and Passivation Approaches

Even though BP provides high mobility, tunable direct bandgap over other 2D materials, it suffers from its instability in ambient conditions, which degrades the device performance with time. This particular stability problem needs to be critically addressed. There are two challenges in addressing BP instability in ambient/water: 1) understanding the degradation mechanism experimentally and theoretically and, 2) exploring alternative approaches to stop/minimize the degradation. It is very clear from the experiments that black phosphorous is unstable and this material degrades in the presence of water and air. Hence, precautions are needed while synthesizing the material or preparing the device. It has been widely adopted to treat few layered BP under vacuum and inert environment, or by minimizing the time of exposing black phosphorous in air, in order to realize its unique properties. Although currently most of the BP devices fabricated in vacuum or inert gas, the devices are required to work in air and ambient atmosphere compatible for many commercial applications.

In terms of the degradation mechanism of BP layers, a few work reported the possible mechanism of the degradation while some work proposed ways to passivate or protect the fabricated devices by avoiding direct contact of black phosphorous with ambient atmosphere. For example, Wood et al. reported by encapsulating the BP with alumina to minimize the material degradation from air/moisture.[190] They examined how exfoliated BP crystals degrade to oxygenated phosphorus compounds in ambient environments. A formation of bubbles on the surface of BP flakes has been observed during the oxidation. They showed that atomic layer deposition (ALD) of AlO_x overlayers is an effective, scalable strategy for passivating BP flakes and FETs from ambient deterioration.[190] **Figure 8**a & 8b shows the BP devices without and with encapsulation on 300 nm thick SiO_2/Si wafer by electron beam lithography with electrodes

consisting of ~2 nm Ti and ~70 nm Au and flakes. AFM height image of a exfoliated BP flake (~9.0 nm thick) exposed in air for 3 days shows large topographic protrusions ("bubbles") above the surface of unprotected BP flake (Figure 8a). The irreversible chemical oxidation of black phosphorous not only can be confirmed by the formation of phosphates but also confirmed by X-ray photoelectron spectroscopy (XPS) spectra noting phosphates.[190] Considerable improvement has been identified for the Hall mobility and on/off ratio of BP FET device over time after encapsulating the devices (Figure 8c). It was reported that, within 6 h of ambient exposure, the FET transfer curve shifts significantly, with the I_{OFF} current increasing by a factor of ~7 and the threshold voltage increasing by 22 V. These observations are attributed to p-type doping from atmospheric adsorbates. The AlO_x encapsulated BP FET was functioning without significant degradation after 1 week of ambient exposure (175 h). Recently a new approach was used to obtain air stable monolayer phosphorene.[191] Oxygen plasma dry etching was used to thin down thick-exfoliated phosphorene flakes layer by layer, and the top layers were oxidized to become P_xO_y, serving as protective layer for the remaining phosphorus underneath together with the following Al_2O_3 passivation layer deposited by ALD.

Transport properties of BP under van der Waals passivation such as graphene and boron nitride on the top of black phosphorus in inert atmosphere was studied by Doganov et al.[44] (Figure 8d & 8e). AFM and Raman spectroscopy measurements were performed on the exposed BP to ambient atmosphere and also for graphene and BN capped BP. AFM height images have been obtained for BP film over time. It is evident that the unprotected surface of the BP film developed significant roughness, while the regions of BP that are under graphene showed no noticeable surface change (Figure 8d & 8e). The time dependence plot showed that the surface roughness drastically improved by BN capping (Figure 8f). Encapsulating BP with graphene and

h-BN seems a promising way to make high performance BP devices. Sandwiched structures of BN/BP/BN have been demonstrated to be highly stable and possess high mobility and on/off ratio (Figure 8g & 8h). These atomically thin BP was completely encapsulated by two BN layers and annealed at temperatures up to 500 °C in an argon atmosphere to further improve the sample quality. Graphene contacted BP transistors are having negligible effect with environment and nearly eliminated hysteresis with stable transport properties (Figure 8i).[154] The encapsulation of suitable 2D thin materials for BP enables for the development of efficient, effective and ultrathin BP field effect transistors.

Electronic-grade BP dispersions were produced with anhydrous organic solvents in a sealed-tip ultrasonication system, which prevents BP degradation that would otherwise occur via solvated O_2 or H_2O.[192] Among conventional solvents, organic solvent NMP is found to provide stable, highly concentrated (~0.4 mg mL^{-1}) BP dispersions. It shows that, using this solvent, the structure and chemistry of solvent-exfoliated BP nanosheets are comparable to mechanically exfoliated BP flakes. Preparing black phosphorous nanosheets in this way will minimize the direct contact of air with BP and show significant performance in the hole mobility and on/off ratio in spite of slightly degradation of BP in organic solvents (not more than 15%).

7. Other Applications

Along with electronic and optoelectronic applications, BP is also getting explored in other applications such as energy storage, van der Waals solids, gas sensing, BP polymer composites and thermoelectric applications due to the development of production and processing techniques for the availability of the material and due to its intrinsic ability for the detection of gases, high aspect ratio nanofiller, high specific capacitance at low voltages and anisotropic character in transport phenomena.

7.1. Energy Storage

Graphene and graphene like TMDs have shown vast potential in energy conversion and storage fields.[193-198] Black phosphorus seems to be another nice material for the application of Li-ion battery.[199-201] Phosphorus is a low-cost abundant material which has high theoretical specific capacity of 2596 mA h g^{-1} in a discharge potential range of 0.4–1.2 V, indicating it's a suitable candidate for anode material.[202] It is known that nanosheets provide higher surface area and specific capacitance compared with their bulk counterparts in battery.[203] Yao and coworkers predicted phosphorene and its nanoribbons can act as fast charging in Li-ion anode materials.[201] According to their studies, phosphorene monolayer and its nanoribbons undergo a transition from semiconductor to metal upon Li adsorption with significant electrons doping to phosphorene. On the other hand, the diffusion of Li atoms in phosphorene shows high anisotropic character and low energy barriers no matter on phosphorene monolayer or nanoribbons. Combining with its electric conductance and optical responses, low diffusion barrier and high anisotropy may be a particular character of phosphorene upon lithiation. Importantly, the moderate binding energy (~2.00 eV) and small migration energy barrier (~0.10 eV along the ZZ direction) of Li atoms on phosphorene make it a potential candidate as an anode material for Li ion batteries. Because of the puckered structure of BP, the diffusion of lithium ions in phosphorene is highly anisotropic in nature. For ions diffusion along ZZ direction, the energy barrier is low (0.08 eV) whereas diffusion along AM direction is almost prohibited. The low energy barrier in phosphorene is significantly low compared with other layered materials such as graphene and MoS_2. DFT calculations reveal that the specific capacity of the phosphorene monolayer is 432.79 mA h g^{-1}, which is larger than those of other commercial anode materials.[204]

Phosphorene is also predicted as a good candidate for Na ion based batteries. Kulish and co-workers performed first principal calculations on Phosphorene in Na ion battery and investigated Na ion diffusion, specific capacity and diffusion mechanism in sodium batteries.[205] Their study revealed that the diffusion of Na ions on phosphorene is fast and anisotropic with the energy barrier of only 0.04 eV. The preliminary data on electrochemistry of black phosphorous experimented by Wang et al.[206] It says that few layer BP is inherently electrochemical active material, meaning that it has redox properties. They have investigated the influence of pH in the range of 2.5-12.5. Recently multilayer BP–graphene based hybrid material as a high-capacity anode for Na-ion batteries was reported.[207] The samples are prepared by simple mixing of liquid dispersions of BP flakes and graphene. It shows 2440 mA h g^{-1} at a current density of 0.05 A g^{-1} and an 83% capacity retention after 100 cycles while operating between 0 and 1.5 V.

7.2. Gas Sensing

2D materials are widely used as chemical gas sensing media.[208-210] Black phosphorous is also sensitive to the surrounding atmosphere which can detect various hazardous gases, ions, vapors, humidity and chemicals. Kou et al. theoretically reported and calculated absorption of CO, CO_2, NH_3, NO, and NO_2 gas molecules on a monolayer phosphorene by studying structural, electronic and transport properties with the edge absorption of toxic gases.[211] They indicated that phosphorene sensing performance can surpass the gas sensing performance of the other 2D materials. Also, gases like NO and NO_2 are having strong affinity towards phosphorene compared with other gases which shows the selectivity of the sensor. Transport calculations revealed that the gas molecule absorption can either increase or decrease the currents which can be measured experimentally. However, their results are completely confined from first-principles calculations. Later, Cui et al. demonstrated FET based gas sensors with high performance using

BP nanosheets towards NO_2 detection at the p.p.b level in dry air.[212] According to their report, the gas sensitivity of the BP FET device depends on the thickness of the nanosheets and 4.8 nm thick device with a sensitivity up to 190% at 20 p.p.b. at room temperature, which showed the best performance. Their FET gas sensor also exhibited high selectivity towards NO_2 gas in the presence of H_2, CO, H_2S gases which corroborates the theoretical support on selectivity of the gas sensing towards NO and NO_2 gases by Kou et al.[211] The higher sensitivity of the gas sensor towards certain gas molecules is due to the changes in the magnitudes of the transport properties when specific gaseous molecule attached to it. NO_2 gas sensing with few layer BP FETs was also performed by Abbas et al.[213] This sensors were sensitive down to the concentration of 5 p.p.b and confirmed that charge transfer is the main mechanism for sensing. The hole conductivity was increased with NO_2 Gas molecules are adsorbed since this molecule withdraws electrons from the BP. Heavy metal ions also effectively detected by a BP gas sensor in a wide concentration range, which shows good air stability due to the encapsulation of BP by a ionophore.[214] The fabricated BP sensors were able to realize multiplex ion detection with excellent selectivity, and sensitive to Pb^{2+} up to 1 ppb. Additionally, the time constant for ion adsorption extracted was only 5 s. BP can also be used to sense the vapor selectively such as methanol vapor[215] and it detected methanol concentration between 380 to 1900 ppm. Additionally, sensitive and selective humidity sensing can be realized using BP film formed by liquid exfoliated flakes.[216, 217] The drain current of such two electrodes sensor increases significantly with the increase of the relative humidity, and the operating principle might be based on the modulation of ionic currents caused by autoionization of water molecules and ionic solvation of the phosphorus oxoacids produced on moist BP surfaces. However, these humidity sensors will degrade as a result of the chemical reaction between humid air and BP flakes.

7.3. Thermoelectric Applications

Thermoelectric (TE) materials can covert directly heat into useful energy, which attracted much interest due to the deployment of fossil fuels and environmental issues. These materials are quantified by a dimensionless Figure of merit ZT which is defined as $ZT = S^2 \frac{\sigma T}{k}$ where S is Seebeck coefficient, σ is the electrical conductivity, T is the absolute temperature, and k is the combination of electronic and lattice thermal conductivity, respectively. It is highly challenging to achieve higher ZT since the transport properties are interlinked and hence limits the performance of the TE device. Given a Seebeck coefficient, two ways can be utilized to enhance the ZT value, namely enlarging electronic conductivity and reducing thermal conductivity, especially reducing the lattice thermal conductivity. Engineering approaches have been made in thermoelectric materials such as Bi_2Te_3/Sb_2Te_3 superlattices with p type and n type doping, nanostructures of bulk alloys $AgPb_mSbTe_{2+m}$, $PbTe_{1-x}Se_x$, Na doped PbTe-SrTe to achieve a higher ZT. The Seebeck coefficient has been measured in the temperature range from 300K to 385 K for black phosphorus, finding a value of S=335+/-10 μV K^{-1} at room temperature (indicating a naturally occurring p-type conductivity).[218] Lv et al predicted that, at the optimal doping level and room temperature, bulk BP and phosphorene have large thermoelectric power factors of 118.4 and 138.9 μWcm^{-1}K^{-2}, respectively.[219] The maximum dimensionless Figure of merit (ZT value) of 0.22 can be achieved in bulk BP by appropriate n-type doping, primarily limited by the reducible lattice thermal conductivity. For the phosphorene, the ZT value can reach 0.30 conservatively estimated by using the bulk lattice thermal conductivity. At the same time, Qin *et al*. investigated the strain effect on the thermoelectric properties of BP.[220] They found that applying strain is a practical way to enhance the thermoelectric performance of BP, and the largest *ZT* value of 0.87 can be achieved at 800 K with a tensile strain of 7%. First-

principles calculations based on DFT showed that the thermoelectric performance of monolayer phosphorene is significantly enhanced by the application of tensile strain along zig-zag direction. Phosphorene subjected to a 10% strain exhibits a very large power factor exceeding 10 mW m^{-1} K^{-2}, which is almost two orders of magnitude greater than the power factors of conventional flexible thermoelectric materials. This extreme enhancement of the thermoelectric performance is explained by the new concept of a strain-induced energy valley.[221]

Zhang et al. show by first-principles calculations that phosphorene nanoribbons (PNRs) with ZZ (ZPNRs) and AM (APNRs) edges have distinct electronic properties, which can be further tuned by hydrogen passivation.[222] Using the Boltzmann theory for both electrons and phonons, the transport coefficients of the PNRs were calculated. As a quick understanding of the thermoelectric performance of such kind of low-dimensional system, the *ZT* value of APNRs and H-passivated ZPNRs with several typical widths are evaluated. Their results indicate that the *ZT* values of APNRs can be optimized to as high as 6.4 at room temperature, which suggests that phosphorene nanoribbons could be very promising candidates for high-performance thermoelectric applications. Qin et al. predict the largest ZT of 0.72 is observed along x direction of bulk BP at temperature of 800 K for an n-type doping concentration of 6.0×10^{19} cm^{-3}, while for the p-type doping, the maximal ZT (0.53) is obtained along the y-direction at 800 K for a hole concentration of 2.72×10^{19} cm^{-3}.[51] ZT may reach the criterion for commercial deployment along the AM direction of phosphorene at T = 500 K and is close to 1 even at room temperature given moderate doping ($\sim2\times10^{16}$ m^{-2}).[139] The largest *ZT* value of 1.65 at 300 K is then conservatively estimated by using the bulk lattice thermal conductivity. When the AM-direction strain of 8% is applied, the room-temperature *ZT* value can reach 2.12 in the AM direction of phosphorene[223] However, most of the papers published in phosphorene for

thermoelectric applications are based on theory and no experimental evidence, so the ZT values discussed above are theoretical predictions due to the lack of chemical method for the production of phosphorene on reliable scale to prepare the samples with alignment of AM and ZZ directions. We hope researchers will focus on towards this point in future.

8. Challenges and Future Outlook

It is a big challenge to invent and discover scalable production methods for single/few layer nanosheets of BP. Production methods are rising up in synthesis, however, it has to compete with other 2D materials production rates. The unprecedented physical properties of single/few layer BP nanosheets are yet to explore in polymer nanocomposites area of research. There are not many applications in using anisotropically physical properties of BP and it needs to be identified. Moreover, it is difficult to make such kind of anisotropy in bulk scale unless there is controllable alignment of nanosheets in certain direction by reproducible method (above millimeter and centimeter scale). Controlling the directional alignment of nanosheets horizontally and vertically on substrates may be an effective method to use the anisotropy of BP. The existing lower on-state current and higher sub-threshold swing could be improved by optimizing gate insulators in the future work in FETs. Another big challenge in few layers BP is to overcome the environmental instability towards oxidation which causes disintegration of phosphorous atoms and hence result in collapse of the device. Currently, it needs to be handled always in vacuum or inter atmospheres to realize its potential though it will be a cost of energy and money. One should find a right molecule to attach to the surface of BP by functionalization without altering much to its physical properties. New methods needs to be developed for scalable production of single/few layer BP nanosheets on grams scale both in dry and liquid state for commercialization applications. Phosphorene oxide might be a feasible solution to prepare in solid state since there

are reduction and exfoliation methods exist for graphene oxide in market. Quantification of strain and spatial distribution is a challenging task. However, it needs to be experimentally verified in phosphorene.

Black phosphorous and its phosphorene nanosheets both are promising candidates in ultra-fast electronics (FET), optoelectronics (Broadband photodetectors and imaging), thermoelectric applications due to its unique puckered structure induced strong anisotropic properties, and its widely tunable bandgap. This material may fill the gap where graphene and other 2D materials compromise to perform. Phosphorene can also be tailored along with other 2D systems such as graphene, MoS_2, WS_2, $MoSe_2$ and ReS_2 in hybrid nanostructures to unravel new physics and new applications in other emerging fields. It will be a long and narrow way to transform phosphorene to technologically feasible and give industrial opportunity.

Acknowledgements

V. Eswaraiah and Q. S. Zeng contributed equally to this manuscript. This work was financially supported by the Singapore National Research Foundation under NRF RF Award No. NRF-RF2013-08, the start-up funding from Nanyang Technological University (M4081137.070) and Singapore Ministry of Education (MOE) Academic Research Fund Tier 1 RG101/13.

Received: ((will be filled in by the editorial staff))
Revised: ((will be filled in by the editorial staff))
Published online: ((will be filled in by the editorial staff))

[1] P. W. Bridgman, *J. Am. Chem. Soc.* **1914**, *36*, 1344.

[2] R. W. Keyes, *Phys. Rev.* **1953**, *92*, 580.

[3] K. S. Novoselov, A. K. Geim, S. V. Morozov, D. Jiang, Y. Zhang, S. V. Dubonos, I. V. Grigorieva, A. A. Firsov, *Science* **2004**, *306*, 666.

[4] Y. Zhu, S. Murali, W. Cai, X. Li, J. W. Suk, J. R. Potts, R. S. Ruoff, *Adv. Mater.* **2010**, *22*, 3906.

[5] J. T. Li, M. C. Lemme, M. Ostling, *Chemphyschem* **2014**, *15*, 3427.

[6] A. C. Ferrari, F. Bonaccorso, V. Fal'ko, K. S. Novoselov, S. Roche, P. Boggild, S. Borini, F. H. L. Koppens, V. Palermo, N. Pugno, J. A. Garrido, R. Sordan, A. Bianco, L. Ballerini, M. Prato, E. Lidorikis, J. Kivioja, C. Marinelli, T. Ryhanen, A. Morpurgo, J. N. Coleman, V. Nicolosi, L. Colombo, A. Fert, M. Garcia-Hernandez, A. Bachtold, G. F. Schneider, F. Guinea, C. Dekker, M. Barbone, Z. Sun, C. Galiotis, A. N. Grigorenko, G. Konstantatos, A. Kis, M. Katsnelson, L. Vandersypen, A. Loiseau, V. Morandi, D. Neumaier, E. Treossi, V. Pellegrini, M. Polini, A. Tredicucci, G. M. Williams, B. Hee Hong, J.-H. Ahn, J. Min Kim, H. Zirath, B. J. van Wees, H. van der Zant, L. Occhipinti, A. Di Matteo, I. A. Kinloch, T. Seyller, E. Quesnel, X. Feng, K. Teo, N. Rupesinghe, P. Hakonen, S. R. T. Neil, Q. Tannock, T. Lofwander, J. Kinaret, *Nanoscale* **2015**, *7*, 4598.

[7] R. H. McKenzie, *Nat. Phys.* **2007**, *3*, 756.

[8] A. K. Geim, K. S. Novoselov, *Nat. Mater.* **2007**, *6*, 183.

[9] H. Liu, A. T. Neal, Z. Zhu, Z. Luo, X. Xu, D. Tomanek, P. D. Ye, *ACS Nano* **2014**, *8*, 4033.

[10] X. Wang, Y. Gong, G. Shi, W. L. Chow, K. Keyshar, G. Ye, R. Vajtai, J. Lou, Z. Liu, E. Ringe, *ACS nano* **2014**, *8*, 5125.

[11] J. Yu, J. Li, W. Zhang, H. Chang, *Chem. Sci.* **2015**, *6*, 6705.

[12] Y. J. Gong, Z. Lin, G. L. Ye, G. Shi, S. M. Feng, Y. Lei, A. L. Elias, N. Perea-Lopez, R. Vajtai, H. Terrones, Z. Liu, M. Terrones, P. M. Ajayan, *Acs Nano* **2015**, *9*, 11658.

[13] X. X. He, F. C. Liu, P. Hu, W. Fu, X. L. Wang, Q. S. Zeng, W. Zhao, Z. Liu, *Small* **2015**, *11*, 5423.

[14] J. Zhou, Q. Zeng, D. Lv, L. Sun, L. Niu, W. Fu, F. Liu, Z. Shen, C. Jin, Z. Liu, *Nano Lett.* **2015**, *15*, 6400.

[15] K. Keyshar, Y. J. Gong, G. L. Ye, G. Brunetto, W. Zhou, D. P. Cole, K. Hackenberg, Y. M. He, L. Machado, M. Kabbani, A. H. C. Hart, B. Li, D. S. Galvao, A. George, R. Vajtai, C. S. Tiwary, P. M. Ajayan, *Adv. Mater.* **2015**, *27*, 4640.

[16] L. Niu, X. Liu, C. Cong, C. Wu, D. Wu, T. R. Chang, H. Wang, Q. Zeng, J. Zhou, X. Wang, *Adv. Mater.* **2015**, *27*, 7800.

[17] A. Castellanos-Gomez, *J. Phys. Chem, Lett.* **2015**, *6*, 4280.

[18] L. Li, Y. Yu, G. J. Ye, Q. Ge, X. Ou, H. Wu, D. Feng, X. H. Chen, Y. Zhang, *Nat. Nanotechnol.* **2014**, *9*, 372.

[19] V. Tran, R. Soklaski, Y. Liang, L. Yang, *Phy. Rev. B* **2014**, *89*, 235319.

[20] Y. Takao, A. Morita, *Physica B & C* **1981**, *105*, 93.

[21] L. B. Liang, J. Wang, W. Z. Lin, B. G. Sumpter, V. Meunier, M. H. Pan, *Nano Lett.* **2014**, *14*, 6400.

[22] Y. Q. Cai, G. Zhang, Y. W. Zhang, *Sci. Rep.* **2014**, *4*, 6677.

[23] J. S. Qiao, X. H. Kong, Z. X. Hu, F. Yang, W. Ji, *Nat. Commun.* **2014**, *5*, 4475.

[24] X. Wang, A. M. Jones, K. L. Seyler, V. Tran, Y. Jia, H. Zhao, H. Wang, L. Yang, X. Xu, F. Xia, *Nat. Nanotechnol.* **2015**, *10*, 517.

[25] F. Guinea, *Solid State Commun.* **2012**, *152*, 1437.

[26] V. M. Pereira, A. H. Castro Neto, *Phys. Rev. Lett.* **2009**, *103*, 046801.

[27] Z. H. Ni, T. Yu, Y. H. Lu, Y. Y. Wang, Y. P. Feng, Z. X. Shen, *ACS Nano* **2008**, *2*, 2301.

[28] A. K. Geim, *Science* **2009**, *324*, 1530.

[29] K. F. Mak, C. Lee, J. Hone, J. Shan, T. F. Heinz, *Phys. Rev. Lett.* **2010**, *105*, 136805.

[30] R. S. Sundaram, M. Engel, A. Lombardo, R. Krupke, A. C. Ferrari, P. Avouris, M. Steiner, *Nano Lett.* **2013**, *13*, 1416.

[31] J. N. Coleman, M. Lotya, A. O'Neill, S. D. Bergin, P. J. King, U. Khan, K. Young, A. Gaucher, S. De, R. J. Smith, I. V. Shvets, S. K. Arora, G. Stanton, H.-Y. Kim, K. Lee, G. T. Kim, G. S. Duesberg, T. Hallam, J. J. Boland, J. J. Wang, J. F. Donegan, J. C. Grunlan, G. Moriarty, A. Shmeliov, R. J. Nicholls, J. M. Perkins, E. M. Grieveson, K. Theuwissen, D. W. McComb, P. D. Nellist, V. Nicolosi, *Science* **2011**, *331*, 568.

[32] Z. Y. Zeng, T. Sun, J. X. Zhu, X. Huang, Z. Y. Yin, G. Lu, Z. X. Fan, Q. Y. Yan, H. H. Hng, H. Zhang, *Angew. Chem. Int. Edit.* **2012**, *51*, 9052.

[33] V. Nicolosi, M. Chhowalla, M. G. Kanatzidis, M. S. Strano, J. N. Coleman, *Science* **2013**, *340*, 1420.

[34] C. L. Tan, P. Yu, Y. L. Hu, J. Z. Chen, Y. Huang, Y. Q. Cai, Z. M. Luo, B. Li, Q. P. Lu, L. H. Wang, Z. Liu, H. Zhang, *J. Am. Chem. Soc.* **2015**, *137*, 10430.

[35] J. Kim, S. S. Baik, S. H. Ryu, Y. Sohn, S. Park, B.-G. Park, J. Denlinger, Y. Yi, H. J. Choi, K. S. Kim, *Science* **2015**, *349*, 723.

[36] R. Fei, V. Tran, L. Yang, *Phy. Rev. B* **2015**, *91*, 195319.

[37] Z. J. Xiang, G. J. Ye, C. Shang, B. Lei, N. Z. Wang, K. S. Yang, D. Y. Liu, F. B. Meng, X. G. Luo, L. J. Zou, Z. Sun, Y. Zhang, X. H. Chen, *Phys. Rev. Lett.* **2015**, *115*, 186403.

[38] Q. H. Liu, X. W. Zhang, L. B. Abdalla, A. Fazzio, A. Zunger, *Nano Lett.* **2015**, *15*, 1222.

[39] S. P. Koenig, R. A. Doganov, H. Schmidt, A. H. C. Neto, B. Ozyilmaz, *Appl. Phys. Lett.* **2014**, *104*, 103106.

[40] L. Li, G. J. Ye, V. Tran, R. Fei, G. Chen, H. Wang, J. Wang, K. Watanabe, T. Taniguchi, L. Yang, X. H. Chen, Y. Zhang, *Nat. Nanotechnol.* **2015**, *10*, 608.

[41] X. Chen, Y. Wu, Z. Wu, Y. Han, S. Xu, L. Wang, W. Ye, T. Han, Y. He, Y. Cai, N. Wang, *Nat. Commun.* **2015**, *6*, 7315.

[42] N. Gillgren, D. Wickramaratne, Y. M. Shi, T. Espiritu, J. W. Yang, J. Hu, J. Wei, X. Liu, Z. Q. Mao, K. Watanabe, T. Taniguchi, M. Bockrath, Y. Barlas, R. K. Lake, C. N. Lau, *2D Mater.* **2015**, *2*, 011001.

[43] Y. Akahama, S. Endo, S.-i. Narita, *J. Phys. Soc. Jpn.* **1983**, *52*, 2148.

[44] R. A. Doganov, E. C. T. O/'Farrell, S. P. Koenig, Y. Yeo, A. Ziletti, A. Carvalho, D. K. Campbell, D. F. Coker, K. Watanabe, T. Taniguchi, A. H. C. Neto, B. Ozyilmaz, *Nat. Commun.* **2015**, *6*, 6647.

[45] M. Engel, M. Steiner, P. Avouris, *Nano Lett.* **2014**, *14*, 6414.

[46] J. Wu, G. K. W. Koon, D. Xiang, C. Han, C. T. Toh, E. S. Kulkarni, I. Verzhbitskiy, A. Carvalho, A. S. Rodin, S. P. Koenig, G. Eda, W. Chen, A. H. C. Neto, B. Özyilmaz, *ACS Nano* **2015**, *9*, 8070.

[47] N. Youngblood, C. Chen, S. J. Koester, M. Li, *Nat. Photonics* **2015**, *9*, 247.

[48] X. Zhang, H. Xie, Z. Liu, C. Tan, Z. Luo, H. Li, J. Lin, L. Sun, W. Chen, Z. Xu, L. Xie, W. Huang, H. Zhang, *Amgew. Chem. Int. Edit* **2015**, *127*, 3724.

[49] R. Fei, L. Yang, *Nano Lett.* **2014**, *14*, 2884.

[50] A. S. Rodin, A. Carvalho, A. H. Castro Neto, *Phys. Rev. Lett.* **2014**, *112*, 176801.

[51] G. Qin, Q.-B. Yan, Z. Qin, S.-Y. Yue, H.-J. Cui, Q.-R. Zheng, G. Su, *Sci. Rep.* **2014**, *4*, 6946.

[52] J.-W. Jiang, H. S. Park, *Nat. Commun.* **2014**, *5*, 4727.

[53] L. Kou, C. Chen, S. C. Smith, *J. Phys. Chem, Lett.* **2015**, *6*, 2794.

[54] H. Liu, Y. Du, Y. Deng, P. D. Ye, *Chem. Soc. Rev.* **2015**, *44*, 2732.

[55] T. T. Shuhei Fukuoka, Toshihito Osada, *J. Phys. Soc. Jpn.* **2015,** *84*, 121004.

[56] S. Balendhran, S. Walia, H. Nili, S. Sriram, M. Bhaskaran, *Small* **2015**, *11*, 640.

[57] Q. Zeng, H. Wang, W. Fu, Y. Gong, W. Zhou, P. M. Ajayan, J. Lou, Z. Liu, *Small* **2015**, *11*, 1868.

[58] H. Du, X. Lin, Z. Xu, D. Chu, *J. Mater. Chem. C* **2015**, *3*, 8760.

[59] S. Lange, P. Schmidt, T. Nilges, *Inorg. Chem.* **2007**, *46*, 4028.

[60] H. Krebs, H. Weitz, K. H. Worms, *Anorg. Allg. Chem.* **1955**, *280*, 119.

[61] A. Brown, S. Rundqvist, *Acta Crystallogr.* **1965**, *19*, 684.

[62] E. Shoichi, A. Yuichi, T. Shin-ichi, N. Shin-ichiro, *Jpn. J. Appl. Phys.* **1982**, *21*, L482.

[63] D. Warschauer, *J. Appl. Phys.* **1963**, *34*, 1853.

[64] S. Narita, Y. Akahama, Y. Tsukiyama, K. Muro, S. Mori, S. Endo, M. Taniguchi, M. Seki, S. Suga, A. Mikuni, H. Kanzaki, *Physica B & C* **1983**, *117*, 422.

[65] Y. Maruyama, S. Suzuki, K. Kobayashi, S. Tanuma, *Physica B & C* **1981**, *105*, 99.

[66] B. Mamoru, I. Fukunori, M. Akira, K. Yoji, F. Tetsuro, *Jpn. J. Appl. Phys.* **1991**, *30*, 1753.

[67] T. Nilges, M. Kersting, T. Pfeifer, *J. Solid State Chem.* **2008**, *181*, 1707.

[68] M. Köpf, N. Eckstein, D. Pfister, C. Grotz, I. Krüger, M. Greiwe, T. Hansen, H. Kohlmann, T. Nilges, *J. Cryst. Growth* **2014**, *405*, 6.

[69] C. A. Di, D. C. Wei, G. Yu, Y. Q. Liu, Y. L. Guo, D. B. Zhu, *Adv. Mater.* **2008**, *20*, 3289.

[70] S. J. Chae, F. Gunes, K. K. Kim, E. S. Kim, G. H. Han, S. M. Kim, H. J. Shin, S. M. Yoon, J. Y. Choi, M. H. Park, C. W. Yang, D. Pribat, Y. H. Lee, *Adv. Mater.* **2009**, *21*, 2328.

[71] V. L. Nguyen, Y. H. Lee, *Small* **2015**, *11*, 3512.

[72] D. Ma, M. Liu, T. Gao, C. Li, J. Sun, Y. Nie, Q. Ji, Y. Zhang, X. Song, Y. Zhang, *Small* **2014**, *10*, 4003.

[73] Y. Xue, B. Wu, Q. Bao, Y. Liu, *Small* **2014**, *10*, 2975.

[74] C. Berger, Z. Song, X. Li, X. Wu, N. Brown, C. Naud, D. Mayou, T. Li, J. Hass, A. N. Marchenkov, E. H. Conrad, P. N. First, W. A. de Heer, *Science* **2006**, *312*, 1191.

[75] P. W. Sutter, J.-I. Flege, E. A. Sutter, *Nat. Mater.* **2008**, *7*, 406.

[76] M. Liu, Y. Gao, Y. Zhang, Y. Zhang, D. Ma, Q. Ji, T. Gao, Y. Chen, Z. Liu, *small* **2013**, *9*, 1360.

[77] G. Huang, T. Chen, W. Chen, Z. Wang, K. Chang, L. Ma, F. Huang, D. Chen, J. Y. Lee, *Small* **2013**, *9*, 3693.

[78] S. Wu, Z. Zeng, Q. He, Z. Wang, S. J. Wang, Y. Du, Z. Yin, X. Sun, W. Chen, H. Zhang, *Small* **2012**, *8*, 2264.

[79] S. Stankovich, D. A. Dikin, R. D. Piner, K. A. Kohlhaas, A. Kleinhammes, Y. Jia, Y. Wu, S. T. Nguyen, R. S. Ruoff, *Carbon* **2007**, *45*, 1558.

[80] Z. Liu, L. Song, S. Zhao, J. Huang, L. Ma, J. Zhang, J. Lou, P. M. Ajayan, *Nano Lett.* **2011**, *11*, 2032.

[81] Z. Liu, L. Ma, G. Shi, W. Zhou, Y. Gong, S. Lei, X. Yang, J. Zhang, J. Yu, K. P. Hackenberg, *Nat. Nanotechnol.* **2013**, *8*, 119.

[82] Q. Feng, Y. Zhu, J. Hong, M. Zhang, W. Duan, N. Mao, J. Wu, H. Xu, F. Dong, F. Lin, *Adv. Mater.* **2014**, *26*, 2648.

[83] Y. J. Gong, J. H. Lin, X. L. Wang, G. Shi, S. D. Lei, Z. Lin, X. L. Zou, G. L. Ye, R. Vajtai, B. I. Yakobson, H. Terrones, M. Terrones, B. K. Tay, J. Lou, S. T. Pantelides, Z. Liu, W. Zhou, P. M. Ajayan, *Nat. Mater.* **2014**, *13*, 1135.

[84] X. D. Duan, C. Wang, J. C. Shaw, R. Cheng, Y. Chen, H. L. Li, X. P. Wu, Y. Tang, Q. L. Zhang, A. L. Pan, J. H. Jiang, R. Q. Yu, Y. Huang, X. F. Duan, *Nat. Nanotechnol.* **2014**, *9*, 1024.

[85] C. M. Huang, S. F. Wu, A. M. Sanchez, J. J. P. Peters, R. Beanland, J. S. Ross, P. Rivera, W. Yao, D. H. Cobden, X. D. Xu, *Nat. Mater.* **2014**, *13*, 1096.

[86] M. Y. Li, Y. M. Shi, C. C. Cheng, L. S. Lu, Y. C. Lin, H. L. Tang, M. L. Tsai, C. W. Chu, K. H. Wei, J. H. He, W. H. Chang, K. Suenaga, L. J. Li, *Science* **2015**, *349*, 524.

[87] J. H. Lee, E. K. Lee, W. J. Joo, Y. Jang, B. S. Kim, J. Y. Lim, S. H. Choi, S. J. Ahn, J. R. Ahn, M. H. Park, C. W. Yang, B. L. Choi, S. W. Hwang, D. Whang, *Science* **2014**, *344*, 286.

[88] X. Ling, H. Wang, S. Huang, F. Xia, M. S. Dresselhaus, *Proc. Natl. Acad. Sci. U.S.A.* **2015**, *112*, 4523.

[89] X. Li, B. Deng, X. Wang, S. Chen, M. Vaisman, S.-i. Karato, G. Pan, M. L. Lee, J. Cha, H. Wang, *2D Mater.* **2015**, *2*, 031002.

[90] Z. Yang, J. Hao, S. Yuan, S. Lin, H. M. Yau, J. Dai, S. P. Lau, *Adv. Mater.* **2015**, *27*, 3748.

[91] Y. Lee, S. Bae, H. Jang, S. Jang, S.-E. Zhu, S. H. Sim, Y. I. Song, B. H. Hong, J.-H. Ahn, *Nano Lett.* **2010**, *10*, 490.

[92] C.-Y. Su, A.-Y. Lu, C.-Y. Wu, Y.-T. Li, K.-K. Liu, W. Zhang, S.-Y. Lin, Z.-Y. Juang, Y.-L. Zhong, F.-R. Chen, L.-J. Li, *Nano Lett.* **2011**, *11*, 3612.

[93] RadisavljevicB, RadenovicA, BrivioJ, GiacomettiV, KisA, *Nat. Nanotechnol.* **2011**, *6*, 147.

[94] K. S. Novoselov, D. Jiang, F. Schedin, T. J. Booth, V. V. Khotkevich, S. V. Morozov, A. K. Geim, *Proc. Natl. Acad. Sci. U.S.A.* **2005**, *102*, 10451.

[95] Y. Cui, R. Xin, Z. Yu, Y. Pan, Z.-Y. Ong, X. Wei, J. Wang, H. Nan, Z. Ni, Y. Wu, T. Chen, Y. Shi, B. Wang, G. Zhang, Y.-W. Zhang, X. Wang, *Adv. Mater.* **2015**, *27*, 5230.

[96] A. O'Neill, U. Khan, J. N. Coleman, *Chem. Mater.* **2012**, *24*, 2414.

[97] G. Cunningham, M. Lotya, C. S. Cucinotta, S. Sanvito, S. D. Bergin, R. Menzel, M. S. P. Shaffer, J. N. Coleman, *ACS Nano* **2012**, *6*, 3468.

[98] D. Hanlon, C. Backes, E. Doherty, C. S. Cucinotta, N. C. Berner, C. Boland, K. Lee, A. Harvey, P. Lynch, Z. Gholamvand, S. Zhang, K. Wang, G. Moynihan, A. Pokle, Q. M. Ramasse, N. McEvoy, W. J. Blau, J. Wang, G. Abellan, F. Hauke, A. Hirsch, S. Sanvito, D. D. O/'Regan, G. S. Duesberg, V. Nicolosi, J. N. Coleman, *Nat. Commun.* **2015**, *6*, 9563.

[99] J. R. Brent, N. Savjani, E. A. Lewis, S. J. Haigh, D. J. Lewis, P. O'Brien, *Chem. Commun.* **2014**, *50*, 13338.

[100] J. Kang, J. D. Wood, S. A. Wells, J. H. Lee, X. L. Liu, K. S. Chen, M. C. Hersam, *Acs Nano* **2015**, *9*, 3596.

[101] P. Yasaei, B. Kumar, T. Foroozan, C. Wang, M. Asadi, D. Tuschel, J. E. Indacochea, R. F. Klie, A. Salehi-Khojin, *Adv. Mater.* **2015**, *27*, 1887.

[102] Z. Guo, H. Zhang, S. Lu, Z. Wang, S. Tang, J. Shao, Z. Sun, H. Xie, H. Wang, X.-F. Yu, P. K. Chu, *Adv. Funct. Mater.* **2015**, 6996.

[103] A. Favron, E. Gaufres, F. Fossard, A. L. Phaneuf-L'Heureux, N. Y. W. Tang, P. L. Levesque, A. Loiseau, R. Leonelli, S. Francoeur, R. Martel, *Nat. Mater.* **2015**, *14*, 826.

[104] J. O. Island, G. A. Steele, H. S. J. van der Zant, A. Castellanos-Gomez, *2D Mater.* **2015**, *2*, 011002.

[105] A. Ziletti, A. Carvalho, D. K. Campbell, D. F. Coker, A. H. C. Neto, *Phys. Rev. Lett.* **2015**, *114*, 046801.

[106] L. Chen, G. Zhou, Z. Liu, X. Ma, J. Chen, Z. Zhang, X. Ma, F. Li, H.-M. Cheng, W. Ren, *Adv. Mater.* **2015**, *28*, 510.

[107] K. R. Paton, E. Varrla, C. Backes, R. J. Smith, U. Khan, A. O'Neill, C. Boland, M. Lotya, O. M. Istrate, P. King, T. Higgins, S. Barwich, P. May, P. Puczkarski, I. Ahmed, M. Moebius, H. Pettersson, E. Long, J. Coelho, S. E. O'Brien, E. K. McGuire, B. M. Sanchez, G. S. Duesberg, N. McEvoy, T. J. Pennycook, C. Downing, A. Crossley, V. Nicolosi, J. N. Coleman, *Nat. Mater.* **2014**, *13*, 624.

[108] E. Varrla, C. Backes, K. R. Paton, A. Harvey, Z. Gholamvand, J. McCauley, J. N. Coleman, *Chem. Mater.* **2015**, *27*, 1129.

[109] E. Varrla, K. R. Paton, C. Backes, A. Harvey, R. J. Smith, J. McCauley, J. N. Coleman, *Nanoscale* **2014**, *6*, 11810.

[110] A. H. Woomer, T. W. Farnsworth, J. Hu, R. A. Wells, C. L. Donley, S. C. Warren, *Acs Nano* **2015**, *9*, 8869.

[111] W. Zhao, Z. Xue, J. Wang, J. Jiang, X. Zhao, T. Mu, *ACS Appl. Mater. Interfaces* **2015**, *7*, 27608.

[112] F. Xia, H. Wang, Y. Jia, *Nat. Commun.* **2014**, *5*, 4458.

[113] A. Morita, *Appl. Phys. A* **1986**, *39*, 227.

[114] R. J. Wu, M. Topsakal, T. Low, M. C. Robbins, N. Haratipour, J. S. Jeong, R. M. Wentzcovitch, S. J. Koester, K. A. Mkhoyan, *J. Vac. Sci. Technol. A* **2015**, *33*, 060604.

[115] Y. Jing, X. Zhang, Z. Zhou, *Wires Comput. Mol. Sci.* **2016**, *6*, 5.

[116] W. L. Lu, H. Y. Nan, J. H. Hong, Y. M. Chen, C. Zhu, Z. Liang, X. Y. Ma, Z. H. Ni, C. H. Jin, Z. Zhang, *Nano Res.* **2014**, *7*, 853.

[117] C.-G. Andres, V. Leonardo, P. Elsa, O. I. Joshua, K. L. Narasimha-Acharya, I. B. Sofya, J. G. Dirk, B. Michele, A. S. Gary, J. V. Alvarez, W. Z. Henny, J. J. Palacios, S. J. v. d. Z. Herre, *2D Mater.* **2014**, *1*, 025001.

[118] J. Wu, N. Mao, L. Xie, H. Xu, J. Zhang, *Amgew. Chem. Int. Edit* **2015**, *127*, 2396.

[119] H. B. Ribeiro, M. A. Pimenta, C. J. S. de Matos, R. L. Moreira, A. S. Rodin, J. D. Zapata, E. A. T. de Souza, A. H. Castro Neto, *ACS Nano* **2015**, *9*, 4270.

[120] J. Kim, J.-U. Lee, J. Lee, H. J. Park, Z. Lee, C. Lee, H. Cheong, *Nanoscale* **2015**, *7*, 18708.

[121] P. H. Tan, W. P. Han, W. J. Zhao, Z. H. Wu, K. Chang, H. Wang, Y. F. Wang, N. Bonini, N. Marzari, N. Pugno, G. Savini, A. Lombardo, A. C. Ferrari, *Nat. Mater.* **2012**, *11*, 294.

[122] H. Zeng, B. Zhu, K. Liu, J. Fan, X. Cui, Q. M. Zhang, *Phy. Rev. B* **2012**, *86*, 241301.

[123] X. Ling, L. Liang, S. Huang, A. A. Puretzky, D. B. Geohegan, B. G. Sumpter, J. Kong, V. Meunier, M. S. Dresselhaus, *Nano Lett.* **2015**, *15*, 4080.

[124] Y. Q. Cai, Q. Q. Ke, G. Zhang, Y. P. Feng, V. B. Shenoy, Y. W. Zhang, *Adv. Funct. Mater.* **2015**, *25*, 2230.

[125] S. Dong, A. Zhang, K. Liu, J. Ji, Y. G. Ye, X. G. Luo, X. H. Chen, X. Ma, Y. Jie, C. Chen, X. Wang, Q. Zhang, *Phys. Rev. Lett.* **2016**, *116*, 087401.

[126] Z.-X. Hu, X. Kong, J. Qiao, B. Normand, W. Ji, *Nanoscale* **2016**, *8*, 2740.

[127] R. Fei, L. Yang, *Appl. Phys. Lett.* **2014**, *105*, 083120.

[128] R. B. Jacobs-Gedrim, M. Shanmugam, N. Jain, C. A. Durcan, M. T. Murphy, T. M. Murray, R. J. Matyi, R. L. Moore, B. Yu, *ACS Nano* **2014**, *8*, 514.

[129] D. J. Late, *ACS Appl. Mater. Interfaces* **2015**, *7*, 5857.

[130] I. Calizo, A. A. Balandin, W. Bao, F. Miao, C. N. Lau, *Nano Lett.* **2007**, *7*, 2645.

[131] S. Sahoo, A. P. S. Gaur, M. Ahmadi, M. J. F. Guinel, R. S. Katiyar, *J. Phys. Chem. C* **2013**, *117*, 9042.

[132] D. J. Late, S. N. Shirodkar, U. V. Waghmare, V. P. Dravid, C. N. R. Rao, *Chemphyschem* **2014**, *15*, 1592.

[133] A. S. Pawbake, J. O. Island, E. Flores, J. R. Ares, C. Sanchez, I. J. Ferrer, S. R. Jadkar, H. S. J. van der Zant, A. Castellanos-Gomez, D. J. Late, *ACS Appl. Mater. Interfaces* **2015**, *7*, 24185.

[134] S. Zhang, J. Yang, R. Xu, F. Wang, W. Li, M. Ghufran, Y.-W. Zhang, Z. Yu, G. Zhang, Q. Qin, Y. Lu, *ACS Nano* **2014**, *8*, 9590.

[135] V. Tran, R. X. Fei, L. Yang, *2D Mater.* **2015**, *2*, 044014.

[136] J. Jin-Wu, *Nanotechnology* **2015**, *26*, 365702.

[137] Z. H. Wang, P. X. L. Feng, *2D Mater.* **2015**, *2*, 021001.

[138] J. Jin-Wu, *Nanotechnology* **2015**, *26*, 055701.

[139] R. Fei, A. Faghaninia, R. Soklaski, J.-A. Yan, C. Lo, L. Yang, *Nano Lett.* **2014**, *14*, 6393.

[140] A. Jain, A. J. H. McGaughey, *Sci. Rep.* **2015**, *5*, 8501.

[141] G. Z. Qin, Q. B. Yan, Z. Z. Qin, S. Y. Yue, M. Hu, G. Su, *Phys. Chem. Chem. Phys.* **2015**, *17*, 4854.

[142] Z.-Y. Ong, Y. Cai, G. Zhang, Y.-W. Zhang, *J. Phys. Chem. C* **2014**, *118*, 25272.

[143] Z. Luo, J. Maassen, Y. Deng, Y. Du, R. P. Garrelts, M. S. Lundstrom, P. D. Ye, X. Xu, *Nat. Commun.* **2015**, *6*, 8572.

[144] S. Lee, F. Yang, J. Suh, S. Yang, Y. Lee, G. Li, H. Sung Choe, A. Suslu, Y. Chen, C. Ko, J. Park, K. Liu, J. Li, K. Hippalgaonkar, J. J. Urban, S. Tongay, J. Wu, *Nat. Commun.* **2015**, *6*, 8573.

[145] H. Jang, J. D. Wood, C. R. Ryder, M. C. Hersam, D. G. Cahill, *Adv. Mater.* **2015**, *27*, 8017.

[146] J. Zhu, J.-Y. Chen, H. Park, X. Gu, H. Zhang, S. Karthikeyan, N. Wendel, S. A. Campbell, M. Dawber, X. Du, M. Li, J.-P. Wang, R. Yang, X. Wang, *Adv. Electron. Mater.* **2016**, DOI: 10.1002/aelm.201600040.

[147] S. Das, M. Demarteau, A. Roelofs, *ACS Nano* **2014**, *8*, 11730.

[148] Y. Du, H. Liu, Y. Deng, P. D. Ye, *ACS Nano* **2014**, *8*, 10035.

[149] S. Das, Z. Wei, L. Raju Thoutam, X. Zhili, A. Hoffmann, M. Demarteau, A. Roelofs, *IEEE Electron Dev. Lett.* **2015**, *36*, 621.

[150] J. Na, Y. T. Lee, J. A. Lim, D. K. Hwang, G. T. Kim, W. K. Choi, Y. W. Song, *Acs Nano* **2014**, *8*, 11753.

[151] D. J. Perello, S. H. Chae, S. Song, Y. H. Lee, *Nat. Commun.* **2015**, *6*, 7809.

[152] H. Wang, X. Wang, F. Xia, L. Wang, H. Jiang, Q. Xia, M. L. Chin, M. Dubey, S.-j. Han, *Nano Lett.* **2014**, *14*, 6424.

[153] G. Long, S. Xu, Z. Wu, T. Han, J. Lin, J. Shen, Y. Han, W. Wong, J. Hou, R. Lortz, *arXiv:1510.06518* **2015**.

[154] A. Avsar, I. J. Vera-Marun, J. Y. Tan, K. Watanabe, T. Taniguchi, A. H. Castro Neto, B. Özyilmaz, *ACS Nano* **2015**, *9*, 4138.

[155] S. Yang, U. K. Chaitanya, C. R. Matthew, H. Nazila, J. K. Steven, *2D Mater.* **2016**, *3*, 011006.

[156] Y. X. Deng, Z. Luo, N. J. Conrad, H. Liu, Y. J. Gong, S. Najmaei, P. M. Ajayan, J. Lou, X. F. Xu, P. D. Ye, *Acs Nano* **2014**, *8*, 8292.

[157] W. Zhu, M. N. Yogeesh, S. Yang, S. H. Aldave, J.-S. Kim, S. Sonde, L. Tao, N. Lu, D. Akinwande, *Nano Lett.* **2015**, *15*, 1883.

[158] Y. Huang, X. F. Duan, C. M. Lieber, *Small* **2005**, *1*, 142.

[159] C. X. Chen, Y. Lu, E. S. Kong, Y. F. Zhang, S. T. Lee, *Small* **2008**, *4*, 1313.

[160] T. Zhai, L. Li, X. Wang, X. Fang, Y. Bando, D. Golberg, *Adv. Funct. Mater.* **2010**, *20*, 4233.

[161] L. J. Yang, S. Wang, Q. S. Zeng, Z. Y. Zhang, T. Pei, Y. Li, L. M. Peng, *Nat. Photonics* **2011**, *5*, 673.

[162] Q. S. Zeng, S. Wang, L. J. Yang, Z. X. Wang, T. Pei, Z. Y. Zhang, L. M. Peng, W. W. Zhou, J. Liu, W. Y. Zhou, S. S. Xie, *Opt. Mater. Express* **2012**, *2*, 839.

[163] G. Konstantatos, M. Badioli, L. Gaudreau, J. Osmond, M. Bernechea, F. P. G. de Arquer, F. Gatti, F. H. L. Koppens, *Nat. Nanotechnol.* **2012**, *7*, 363.

[164] Q. H. Wang, K. Kalantar-Zadeh, A. Kis, J. N. Coleman, M. S. Strano, *Nat. Nanotechnol.* **2012**, *7*, 699.

[165] L. J. Yang, S. Wang, Q. S. Zeng, Z. Y. Zhang, L. M. Peng, *Small* **2013**, *9*, 1225.

[166] D. Kufer, I. Nikitskiy, T. Lasanta, G. Navickaite, F. H. Koppens, G. Konstantatos, *Adv. Mater.* **2015**, *27*, 176.

[167] O. Lopez-Sanchez, D. Lembke, M. Kayci, A. Radenovic, A. Kis, *Nat Nano* **2013**, *8*, 497.

[168] F. H. L. Koppens, T. Mueller, P. Avouris, A. C. Ferrari, M. S. Vitiello, M. Polini, *Nat. Nanotechnol.* **2014**, *9*, 780.

[169] A. Abderrahmane, P. J. Ko, T. V. Thu, S. Ishizawa, T. Takamura, A. Sandhu, *Nanotechnology* **2014**, *25*, 365202.

[170] F. Liu, H. Shimotani, H. Shang, T. Kanagasekaran, V. Zólyomi, N. Drummond, V. I. Fal'ko, K. Tanigaki, *ACS Nano* **2014**, *8*, 752.

[171] P. Yu, X. Yu, W. Lu, H. Lin, L. Sun, K. Du, F. Liu, W. Fu, Q. Zeng, Z. Shen, *Adv. Funct. Mater.* **2016**, *26*, 137.

[172] J. Schornbaum, B. Winter, S. P. Schießl, F. Gannott, G. Katsukis, D. M. Guldi, E. Spiecker, J. Zaumseil, *Adv. Funct. Mater.* **2014**, *24*, 5798.

[173] C. X. Guo, H. B. Yang, Z. M. Sheng, Z. S. Lu, Q. L. Song, C. M. Li, *Angew. Chem. Int. Edit.* **2010**, *49*, 3014.

[174] M. Baba, Y. Takeda, K. Shibata, T. Ikeda, A. Morita, *Jpn. J. Appl. Phys.* **1989**, *28*, L2104.

[175] M. Buscema, D. J. Groenendijk, S. I. Blanter, G. A. Steele, H. S. J. van der Zant, A. Castellanos-Gomez, *Nano Lett.* **2014**, *14*, 3347.

[176] M. Buscema, D. J. Groenendijk, G. A. Steele, H. S. J. van der Zant, A. Castellanos-Gomez, *Nat. Commun.* **2014**, *5*, 4651.

[177] T. Low, M. Engel, M. Steiner, P. Avouris, *Phy. Rev. B* **2014**, *90*, 081408.

[178] Z. Yin, H. Li, H. Li, L. Jiang, Y. Shi, Y. Sun, G. Lu, Q. Zhang, X. Chen, H. Zhang, *ACS Nano* **2012**, *6*, 74.

[179] W. Choi, M. Y. Cho, A. Konar, J. H. Lee, G.-B. Cha, S. C. Hong, S. Kim, J. Kim, D. Jena, J. Joo, S. Kim, *Adv. Mater.* **2012**, *24*, 5832.

[180] N. Perea-López, A. L. Elías, A. Berkdemir, A. Castro-Beltran, H. R. Gutiérrez, S. Feng, R. Lv, T. Hayashi, F. López-Urías, S. Ghosh, B. Muchharla, S. Talapatra, H. Terrones, M. Terrones, *Adv. Funct. Mater.* **2013**, *23*, 5511.

[181] P. Hu, Z. Wen, L. Wang, P. Tan, K. Xiao, *Acs Nano* **2012**, *6*, 5988.

[182] P. Hu, L. Wang, M. Yoon, J. Zhang, W. Feng, X. Wang, Z. Wen, J. C. Idrobo, Y. Miyamoto, D. B. Geohegan, K. Xiao, *Nano Lett.* **2013**, *13*, 1649.

[183] T. Hong, B. Chamlagain, W. Z. Lin, H. J. Chuang, M. H. Pan, Z. X. Zhou, Y. Q. Xu, *Nanoscale* **2014**, *6*, 8978.

[184] H. Yuan, X. Liu, F. Afshinmanesh, W. Li, G. Xu, J. Sun, B. Lian, A. G. Curto, G. Ye, Y. Hikita, Z. Shen, S.-C. Zhang, X. Chen, M. Brongersma, H. Y. Hwang, Y. Cui, *Nat. Nanotechnol.* **2015**, *10*, 707.

[185] L. Viti, J. Hu, D. Coquillat, W. Knap, A. Tredicucci, A. Politano, M. S. Vitiello, *Adv. Mater.* **2015**, *27*, 5567.

[186] Y. Deng, N. J. Conrad, Z. Luo, H. Liu, X. Xu, P. D. Ye, in *Electron Devices Meeting (IEDM)*, 2014 IEEE International, IEEE: **2014**; pp 5.2. 1.

[187] M. V. Kamalakar, B. N. Madhushankar, A. Dankert, S. P. Dash, *Small* **2015**, *11*, 2209.

[188] K. Gong, L. Zhang, W. Ji, H. Guo, *Phy. Rev. B* **2014**, *90*, 125441.

[189] M. Huang, M. Wang, C. Chen, Z. Ma, X. Li, J. Han, Y. Wu, *Adv. Mater.* **2016**, DOI: 10.1002/adma.201506352.

[190] J. D. Wood, S. A. Wells, D. Jariwala, K.-S. Chen, E. Cho, V. K. Sangwan, X. Liu, L. J. Lauhon, T. J. Marks, M. C. Hersam, *Nano Lett.* **2014**, *14*, 6964.

[191] J. Pei, X. Gai, J. Yang, X. Wang, Z. Yu, D.-Y. Choi, B. Luther-Davies, Y. Lu, *Nat. Commun.* **2016**, *7*, 10450.

[192] J. Kang, J. D. Wood, S. A. Wells, J.-H. Lee, X. Liu, K.-S. Chen, M. C. Hersam, *ACS Nano* **2015**, *9*, 3596.

[193] Z. Niu, J. Du, X. Cao, Y. Sun, W. Zhou, H. H. Hng, J. Ma, X. Chen, S. Xie, *Small* **2012**, *8*, 3201.

[194] S. Han, D. Q. Wu, S. Li, F. Zhang, X. L. Feng, *Small* **2013**, *9*, 1173.

[195] L. J. Cao, S. B. Yang, W. Gao, Z. Liu, Y. J. Gong, L. L. Ma, G. Shi, S. D. Lei, Y. H. Zhang, S. T. Zhang, R. Vajtai, P. M. Ajayan, *Small* **2013**, *9*, 2905.

[196] Z. Q. Niu, L. Zhang, L. Liu, B. W. Zhu, H. B. Dong, X. D. Chen, *Adv. Mater.* **2013**, *25*, 4035.

[197] L. L. Liu, Z. Q. Niu, L. Zhang, W. Y. Zhou, X. D. Chen, S. S. Xie, *Adv. Mater.* **2014**, *26*, 4855.

[198] H. Wang, H. B. Feng, J. H. Li, *Small* **2014**, *10*, 2165.

[199] C. M. Park, H. J. Sohn, *Adv. Mater.* **2007**, *19*, 2465.

[200] W. Li, Y. Yang, G. Zhang, Y.-W. Zhang, *Nano Lett.* **2015**, *15*, 1691.

[201] Q. Yao, C. Huang, Y. Yuan, Y. Liu, S. Liu, K. Deng, E. Kan, *J. Phys. Chem. C* **2015**, *119*, 6923.

[202] J. Sun, G. Zheng, H.-W. Lee, N. Liu, H. Wang, H. Yao, W. Yang, Y. Cui, *Nano Lett.* **2014**, *14*, 4573.

[203] Y. Liu, M. Zhu, D. Chen, *J. Mater. Chem. A* **2015**, *3*, 11862.

[204] S. Zhao, W. Kang, J. Xue, *J. Mater. Chem. A* **2014**, *2*, 19046.

[205] V. V. Kulish, O. I. Malyi, C. Persson, P. Wu, *Phys. Chem. Chem. Phys.* **2015**, 17, 13921.

[206] L. Wang, Z. Sofer, M. Pumera, *ChemElectroChem* **2015**, *2*, 324.

[207] J. Sun, H.-W. Lee, M. Pasta, H. Yuan, G. Zheng, Y. Sun, Y. Li, Y. Cui, *Nat. Nanotechnol.* **2015**, *10*, 980.

[208] B. Cho, J. Yoon, S. K. Lim, A. R. Kim, D. H. Kim, S. G. Park, J. D. Kwon, Y. J. Lee, K. H. Lee, B. H. Lee, H. C. Ko, M. G. Hahm, *ACS Appl. Mater. Interfaces* **2015**, *7*, 16775.

[209] Y. H. Kim, S. J. Kim, Y.-J. Kim, Y.-S. Shim, S. Y. Kim, B. H. Hong, H. W. Jang, *ACS nano* **2015**, *9*, 10453.

[210] C. C. Mayorga-Martinez, A. Ambrosi, A. Y. S. Eng, Z. Sofer, M. Pumera, *Adv. Funct. Mater.* **2015**, *25*, 5611.

[211] L. Kou, T. Frauenheim, C. Chen, *J. Phys. Chem, Lett.* **2014**, *5*, 2675.

[212] S. Cui, H. Pu, S. A. Wells, Z. Wen, S. Mao, J. Chang, M. C. Hersam, J. Chen, *Nat. Commun.* **2015**, *6*, 8632.

[213] A. N. Abbas, B. Liu, L. Chen, Y. Ma, S. Cong, N. Aroonyadet, M. Köpf, T. Nilges, C. Zhou, *ACS Nano* **2015**, *9*, 5618.

[214] P. Li, D. Zhang, J. Liu, H. Chang, Y. e. Sun, N. Yin, *ACS Appl. Mater. Interfaces* **2015**, *7*, 24396.

[215] C. C. Mayorga-Martinez, Z. Sofer, M. Pumera, *Amgew. Chem. Int. Edit* **2015**, *54*, 14317.

[216] P. Yasaei, A. Behranginia, T. Foroozan, M. Asadi, K. Kim, F. Khalili-Araghi, A. Salehi-Khojin, *Acs Nano* **2015**, *9*, 9898.

[217] D. J. Late, *Micropor. Mesopor. Mat.* **2016**, *225*, 494.

[218] E. Flores, J. R. Ares, A. Castellanos-Gomez, M. Barawi, I. J. Ferrer, C. Sánchez, *Appl. Phys. Lett.* **2015**, *106*, 022102.

[219] H. Lv, W. Lu, D. Shao, Y. Sun, *arXiv:1404.5171* **2014**.

[220] G. Z. Qin, Q. B. Yan, Z. Z. Qin, S. Y. Yue, H. J. Cui, Q. R. Zheng, G. Su, *Sci. Rep.* **2014**, *4*, 6946.

[221] K. Satoru, Y. Takahiro, *Appl. Phys. Express* **2015**, *8*, 015202.

[222] J. Zhang, H. J. Liu, L. Cheng, J. Wei, J. H. Liang, D. D. Fan, J. Shi, X. F. Tang, Q. J. Zhang, *Sci. Rep.* **2014**, *4*, 6452.

[223] H. Y. Lv, W. J. Lu, D. F. Shao, Y. P. Sun, *Phy. Rev. B* **2014**, *90*, 085433.

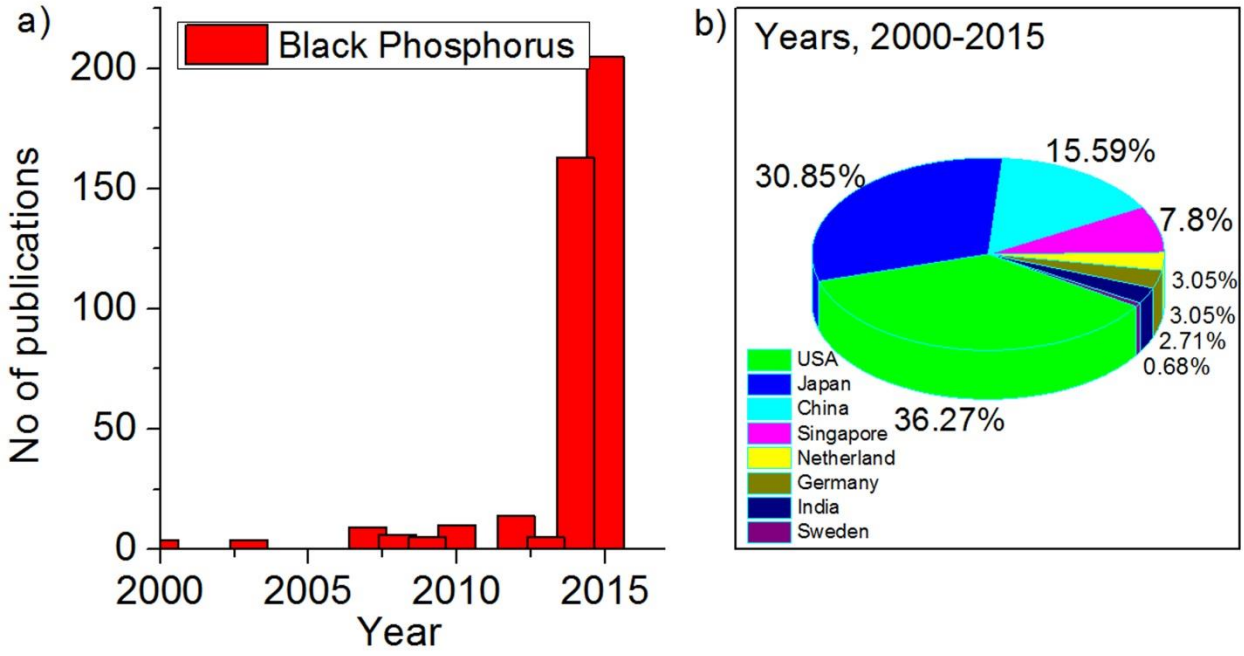

Figure 1. Articles Published in Phosphorus across the globe: a) Number of articles published in black phosphorous from 2000-2015 (search keyword "Black Phosphorus" on 04/12/2015). b) Pie chart describing number of articles published by different countries across the globe (data retrieved from Sci finder).

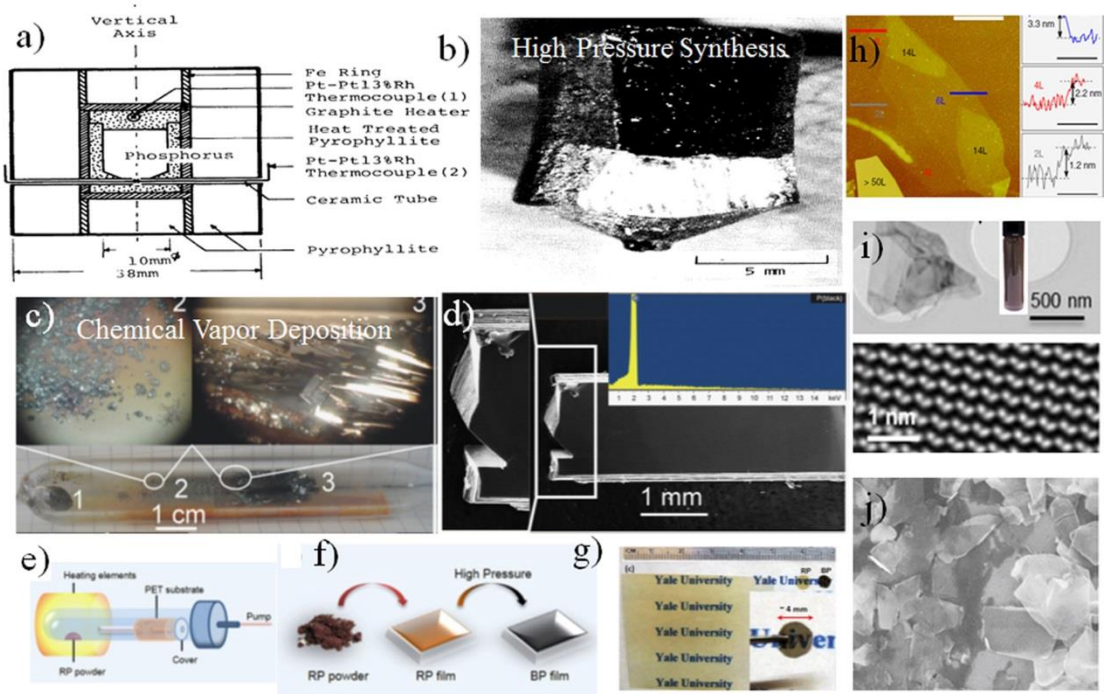

Figure 2. Synthesis of BP crystal and nanosheets. a) A cross section of cubic cell designed for growth of black phosphorus (BP) crystal at high pressure and high temperatures. b) An ingot of obtained BP crystal shows clear faces. (a-b) Reproduced with permission.[62] Copyright 1982, IOP publishing. c) Chemical Vapor transport reaction converting red phosphorus into black phosphorus (1) and d) different portions of the sample in magnified view (2, 3, 4). (c-d) Reproduced with permission.[59] Copyright 2007, American chemical Society. e) Strategy for the synthesis of thin BP films. (f) Schematic apparatus for the deposition of RP film. (g) Photos of thin red phosphorus (RP) film on PET substrate (left), RP/PET disc for pressurization (middle) and BP/PET disc after pressurization. The inset shows the transparency of the BP/PET film. (e-g) Reproduced with permission.[89] Copyright 2015, IOP publishing. h) Micromechanically exfoliated BP flake showing 6L, 14L, 50L and >50L by contrast difference and AFM profile of 2L, 4L and 6L of BP. Reproduced with permission.[112] Copyright 2014, Nature Publishing Group. i) liquid phase exfoliated and few layered BP in organic solvent (inset: BP in CHP) and high resolution micrograph of puckered black phosphorous demonstrates the corrugation on its surface. j) Random distribution of BP flakes few layered in SEM image demonstrates it can be exfoliated in bulk scale. (i-j) Reproduced with permission.[98] Copyright 2015, Nature Publishing Group.

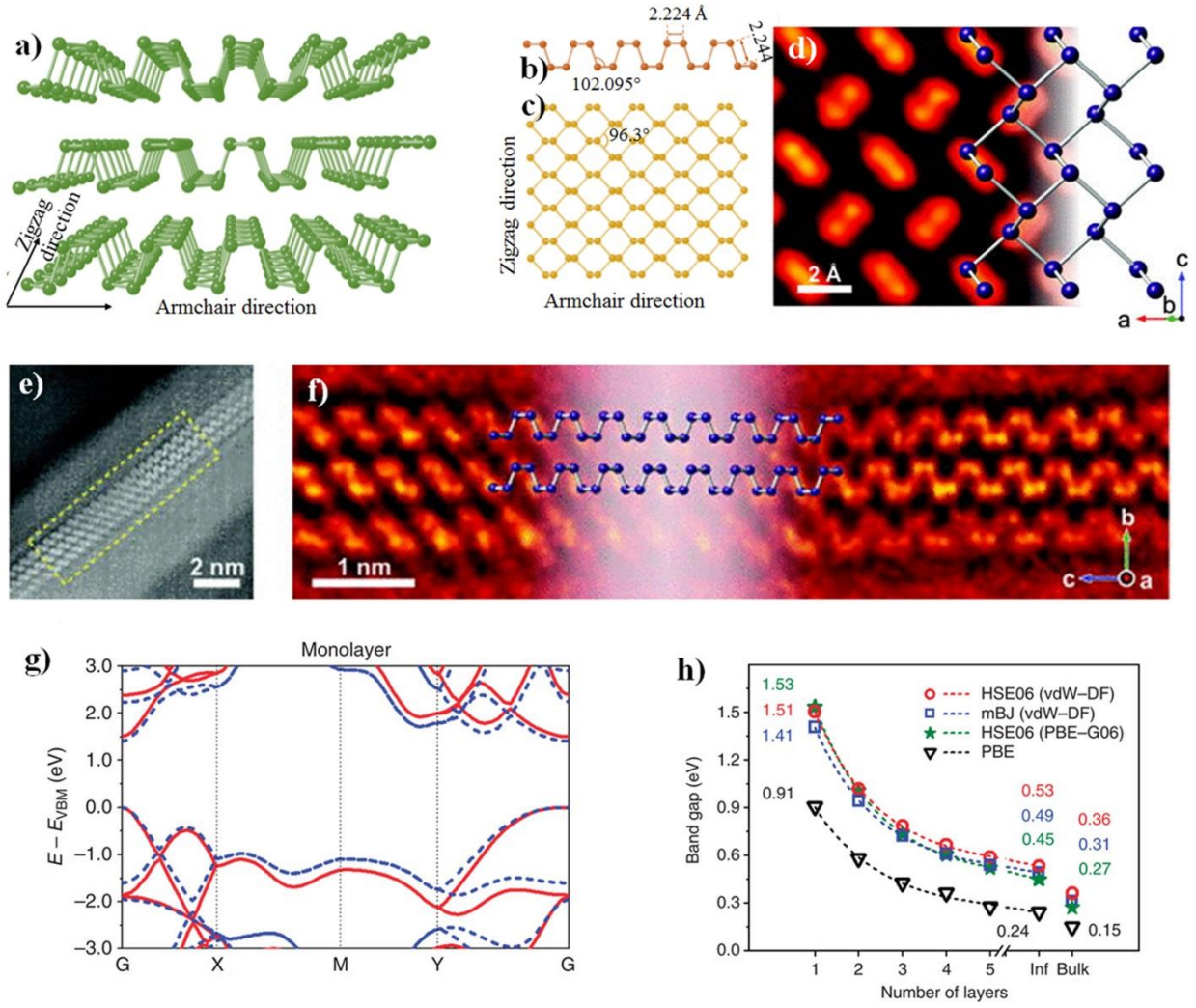

Figure 3. Structural view of BP. (a) Atomic structure of multi-layer black phosphorus and (b) monolayer phosphorene from side view, c) top view. (a-c) Reproduced with permission.[58] Copyright 2015, Royal society of chemistry. d) ADF-STEM image viewed along the [101] direction or 17° tilted off the [001] zone axis. e) ADF-STEM image captured at an edge of a BP flake showing multiple layers stacked together, or along the [100] direction. f) Magnified image of the region highlighted in (e). (d-f) Reproduced with permission.[114] Copyright 2015, AIP Publishing. g) Bandstructures of monolayer BP calculated with the HSE06 functional (red solid lines) and the mBJ potential (blue dashed lines), respectively. h) Evolution of the direct bandgaps as a function of the sample thickness. (g-h) Reproduced with permission.[23] Copyright 2014, Nature publishing group.

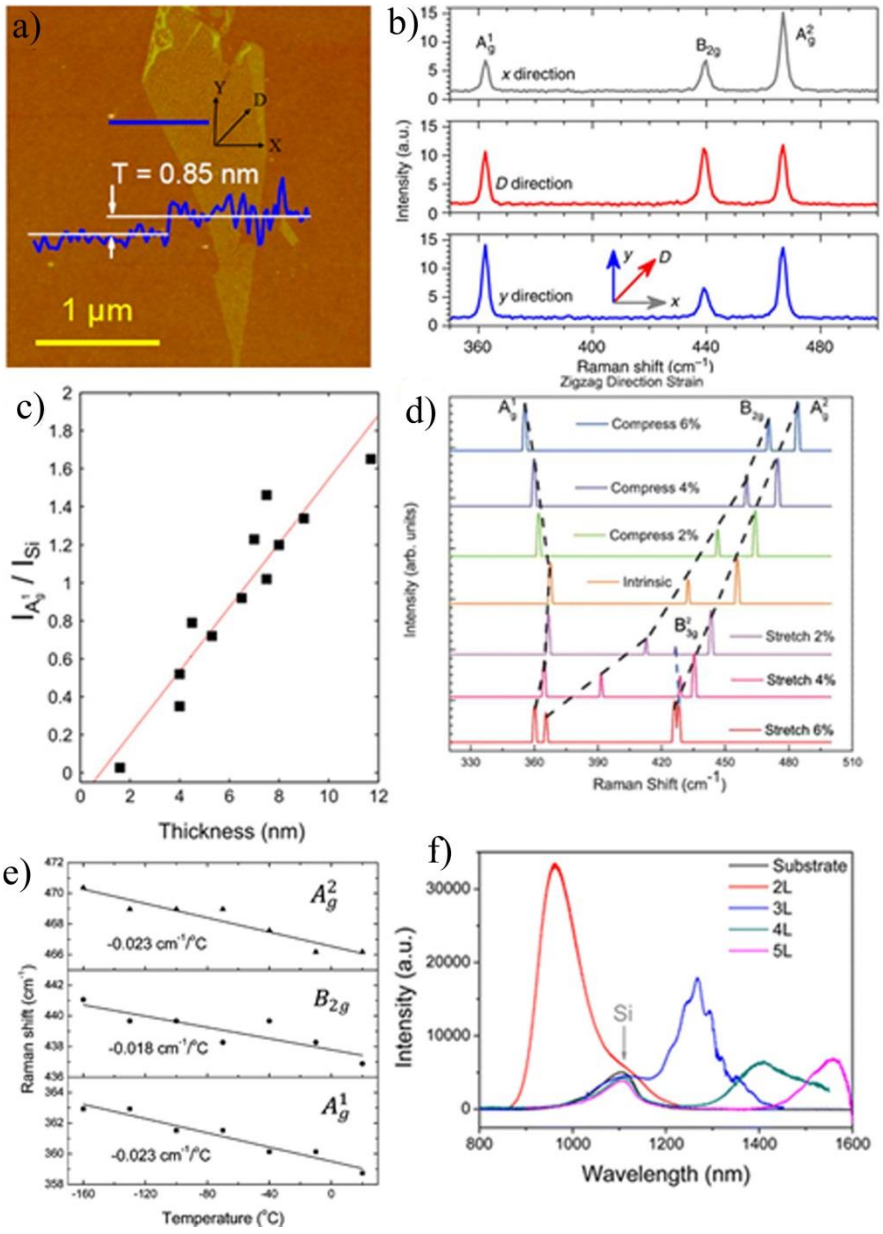

Figure 4. Spectroscopic characterization of Black Phosphorus. a) AFM image of exfoliated few layered BP crystal with sectional profile displaying 0.85 nm. Reproduced with permission.[9] Copyright 2014, American Chemical Society. b) Polarization-resolved Raman spectra of a BP layered thin film with 532-nm linearly polarized laser excitation incident in the *z* direction. Raman spectra with excitation laser polarization along *x*- (grey), *D*- (red) and *y* directions (blue). The *D* direction is along 45° angle relative to the *x*- and *y* directions, as shown in the bottom

panel. Reproduced with permission.[112] Copyright 2014, Nature publishing group. c) Thickness dependence of the intensity ratio between the A_g^1 and Si peaks. Reproduced with permission.[117] Copyright 2014, IOP publishing. d) Raman spectra of phosphorene under uniaxial strain along ZZ direction. Reproduced with permission.[127] Copyright 2014, AIP publishing. e) Temperature dependence of A_g^1, B_{2g}, and A_g^2 Raman peak positions and f) PL spectra of 2L, 3L, 4L, and 5L BP flakes. (e-f) Reproduced with permission.[128] Copyright 2014, American chemical society.

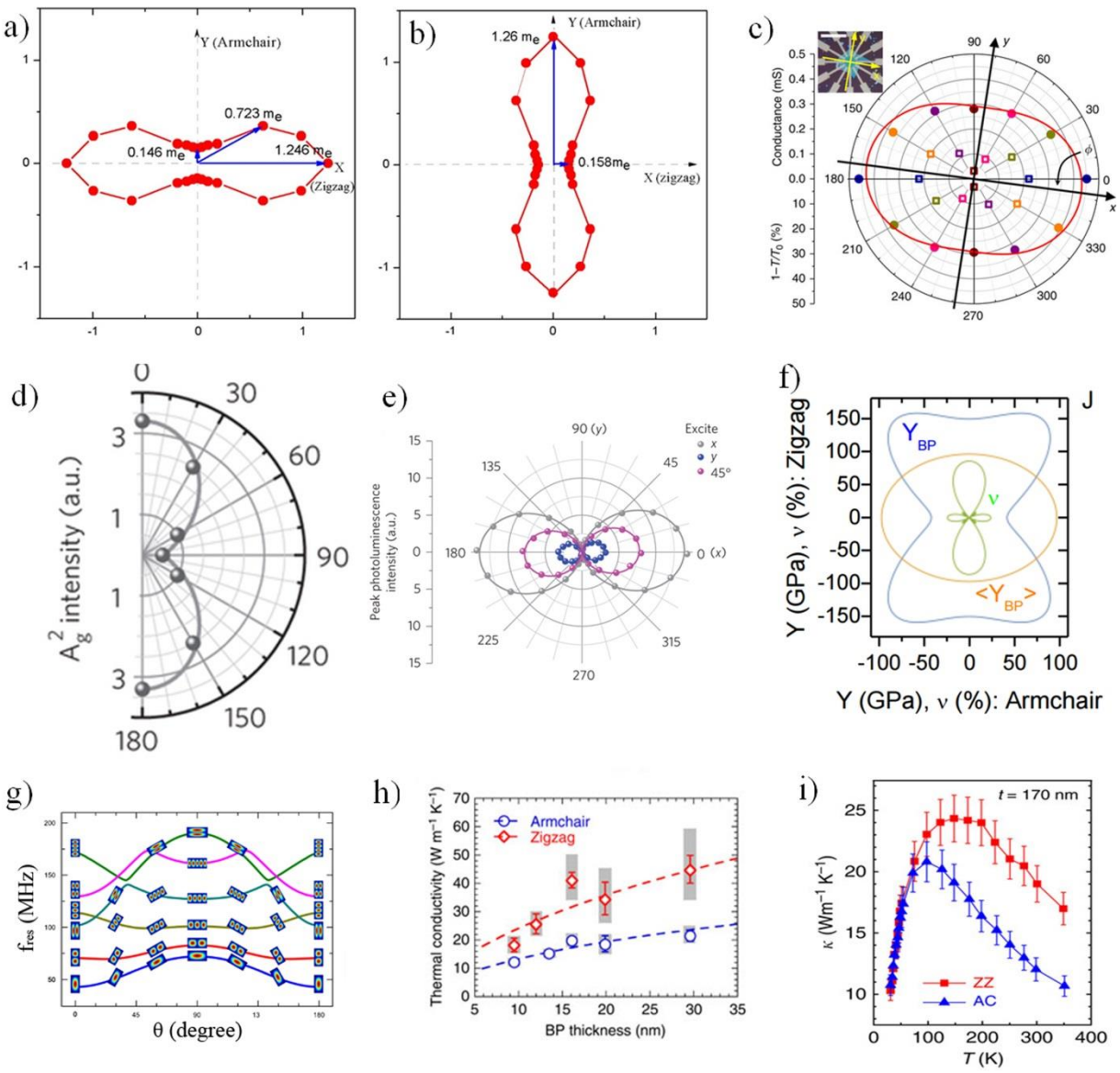

Figure 5. Anisotropic characteristics of BP. a) Electron effective mass according to the spatial direction that of intrinsic phosphorene and (b) 5% biaxially strained phosphorene. (a-b) Reproduced with permission.[49] Copyright 2014, American chemical society. c) The angle-resolved DC conductance (solid dots) and the polarization-resolved relative extinction of the same flake at 2,700 cm^{-1} (hollow squares) in polar plot, Inset: an optical image of this BP flake. Scale bar: 50 μm. Reproduced with permission.[112] Copyright 2014, Nature publishing group. d) Intensity of the A_g^2 mode as a function of the excitation laser polarization angle in the *x*–*y* plane. e) Photoluminescence peak intensity as a function of polarization detection angle for excitation laser polarized along *x* (grey), 45° (magenta) and *y* (blue) directions. Reproduced with

permission.[24] Copyright 2015, Nature publishing group. f) Calculated orientation-dependence of the bulk BP in-plane-only Young's modulus (blue), its hill average (yellow) and Poisson's ratio (green). Reproduced with permission.[98] Copyright, 2015, Nature publishing group. g) The f_{res} and mode shapes for the first six modes are shown for 5 × 10 μm rectangular black P resonators with $t = 200$ nm as functions of the orientation angle θ. Reproduced with permission[137] Copyright 2015, IOP publishing. h) AM and ZZ in-plane thermal conductivities of BP films vs. thickness. Reproduced with permission.[143] Copyright 2015, Nature publishing group. i) Thermal conductivity versus temperature plot of BP nanoribbons axially oriented to the ZZ and AC directions. Reproduced with permission.[144] Copyright 2015, Nature publishing group.

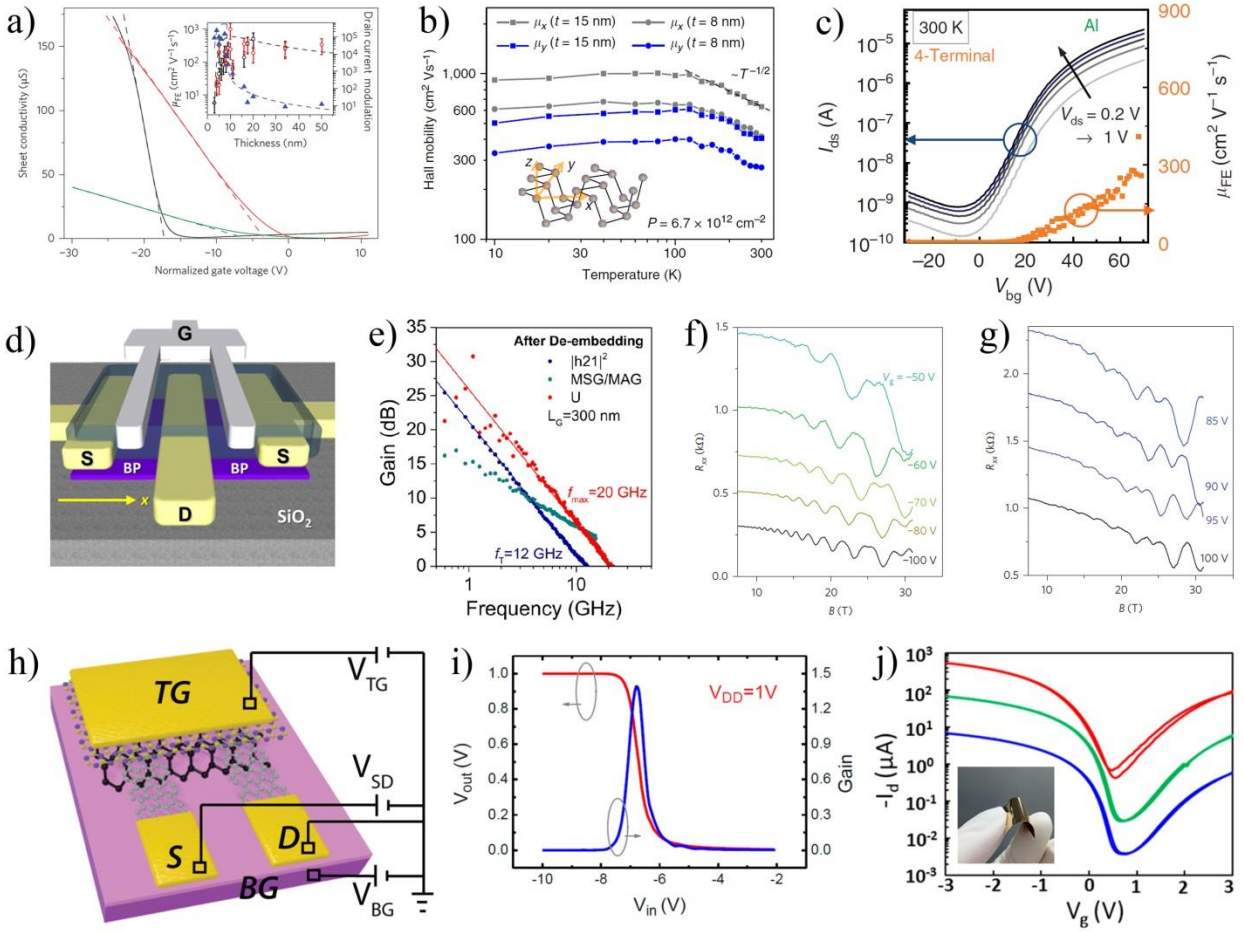

Figure 6. Electronic devices of BP. a) Sheet conductivity measured as a function of gate voltage for devices with different thicknesses: 10 nm (black solid line), 8 nm (red solid line), and 5 nm (green solid line), with field-effect mobility values of 984 $cm^2 \cdot V^{-1} \cdot s^{-1}$, 197 $cm^2 \cdot V^{-1} \cdot s^{-1}$, and 55 $cm^2 \cdot V^{-1} \cdot s^{-1}$, respectively, and inset are field-effect mobilities extracted from the line fit of the linear region of the conductivity (dashed lines). Reproduced with permission.[18] Copyright 2014, Nature Publishing Group. b) Angle-resolved Hall mobility vs. temperature, and inset is schematic view of a single-layer black P showing different crystalline directions. Reproduced with permission.[112] Copyright 2014, Nature Publishing Group. c) Alluminium-contacted n-type BP FET operating with a $I_{on}/I_{off} \sim 10^5$ at 300 K, and the 4-terminal-calculated electron mobility at 300 K is 275 cm^2V^{-1} s^{-1}. Reproduced with permission.[151] Copyright 2015, Nature Publishing Group. d) Schematic of BP high-frequency transistor. e) The short-circuit current gain h_{21}, maximum stable gain (MSG)/maximum available gain (MAG), and unilateral power gain U of the 300-nm channel length device after de-embedding. (d-e) Reproduced with permission.[152] Copyright 2014, American Chemical Society. f)-g) R_{xx} of BP placed on h-BN substrate as a function of magnetic field measured at varying gate voltages. SdH oscillations are observed for both holes f) and electrons g) at T = 0.3 K. (f-g) Reproduced with permission.[40] Copyright 2015, Nature Publishing Group. h) The schematic of graphene contacted and *h*-BN encapsulated BP FET together with the electrical connections. Reproduced with permission.[154] Copyright 2015, American Chemical Society. i) Voltage transfer curve V_{out} (V_{in}) and gain of the 2D CMOS inverter consisting BP PMOS and MoS_2 NMOS. Reproduced with permission.[9] Copyright 2014, American Chemical Society. j) Transfer characteristics of encapsulated BP FET on PI with a drain bias V_d = −10 mV, −100 mV and −1 V from bottom to top. Reproduced with permission.[157] Copyright 2015, American Chemical Society.

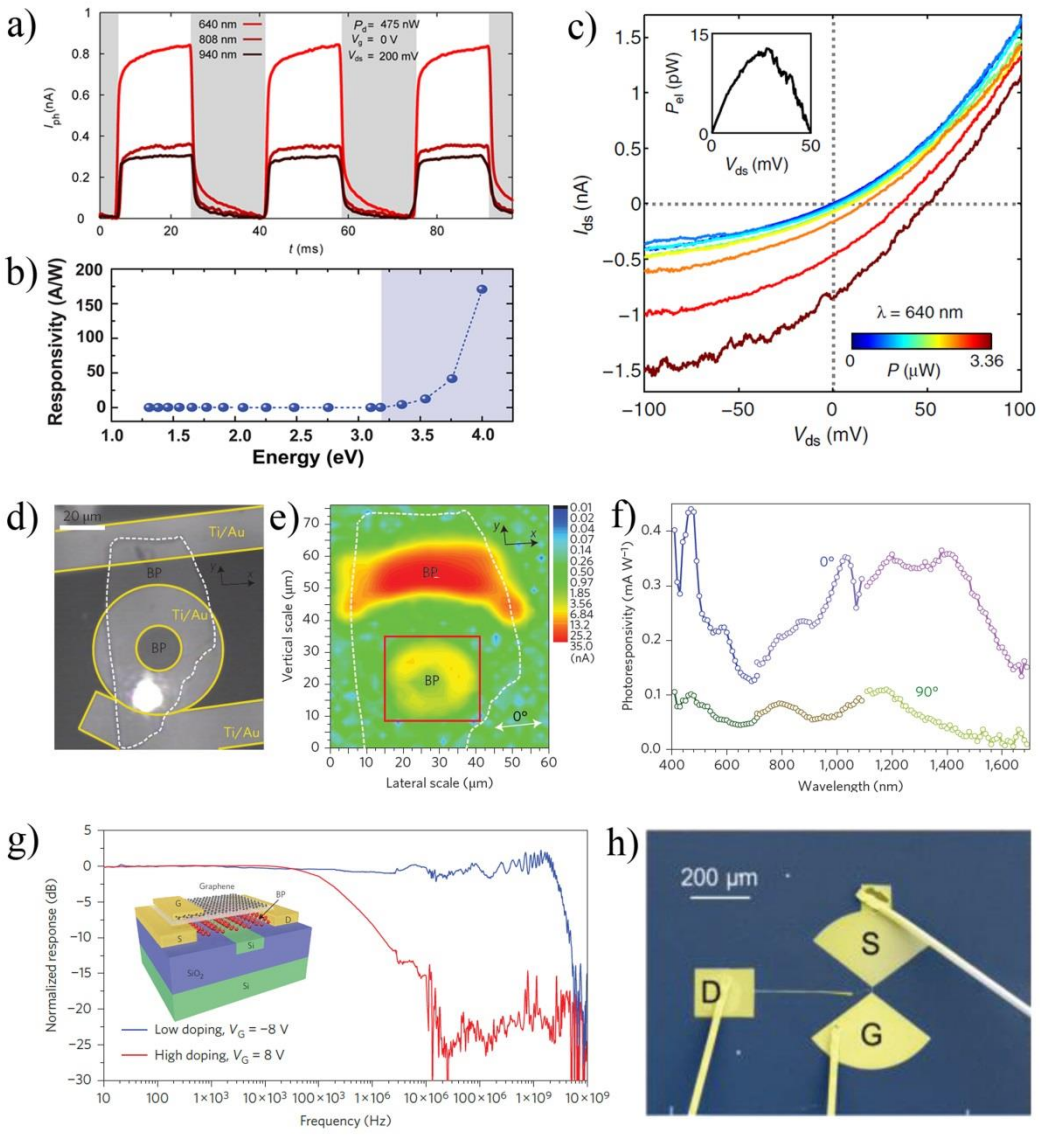

Figure 7. BP photodetector. a) Photocurrent of BP FET as a function of time under modulated light excitation (~20 Hz) with different wavelengths. Reproduced with permission.[175] Copyright 2014, American Chemical Society. b) Photoresponsivity of BP FET within the energy range 1−4 eV measured at V_{BG} = -80 V and V_{SD} = 0.1 V. Reproduced with permission.[46] Copyright 2015, American Chemical Society. c) Output characteristics in the PN configuration as a function of the incident optical power (640 nm). The inset shows the electrical power that can be harvested at the maximum employed illumination power. Reproduced with permission.[176] Copyright 2014, Nature Publishing Group. d) Optical image of a BP photodetector with a ring-shaped photocurrent collector. e) Corresponding photocurrent microscopy image of the device

shown in d with illumination at 1500 nm and polarization along the x direction. f) Polarization dependence of photoresponsivity with illumination from 400 to 1700 nm, where the polarization angle of 0° corresponds to the x crystal axis and 90° corresponds to the y crystal axis. (d-f) Reproduced with permission.[184] Copyright 2015, Nature Publishing Group. g) The response of the BP photodetector is measured when the BP is gated to low and high doping, resulting in a cutoff frequency of 3 GHz and 0.2 MHz respectively. Reproduced with permission.[47] Copyright 2015, Nature Publishing Group. h) Optical image of BP terahertz photodetector with planar bow-tie antenna design. Reproduced with permission.[185] Copyright 2015, Wiley.

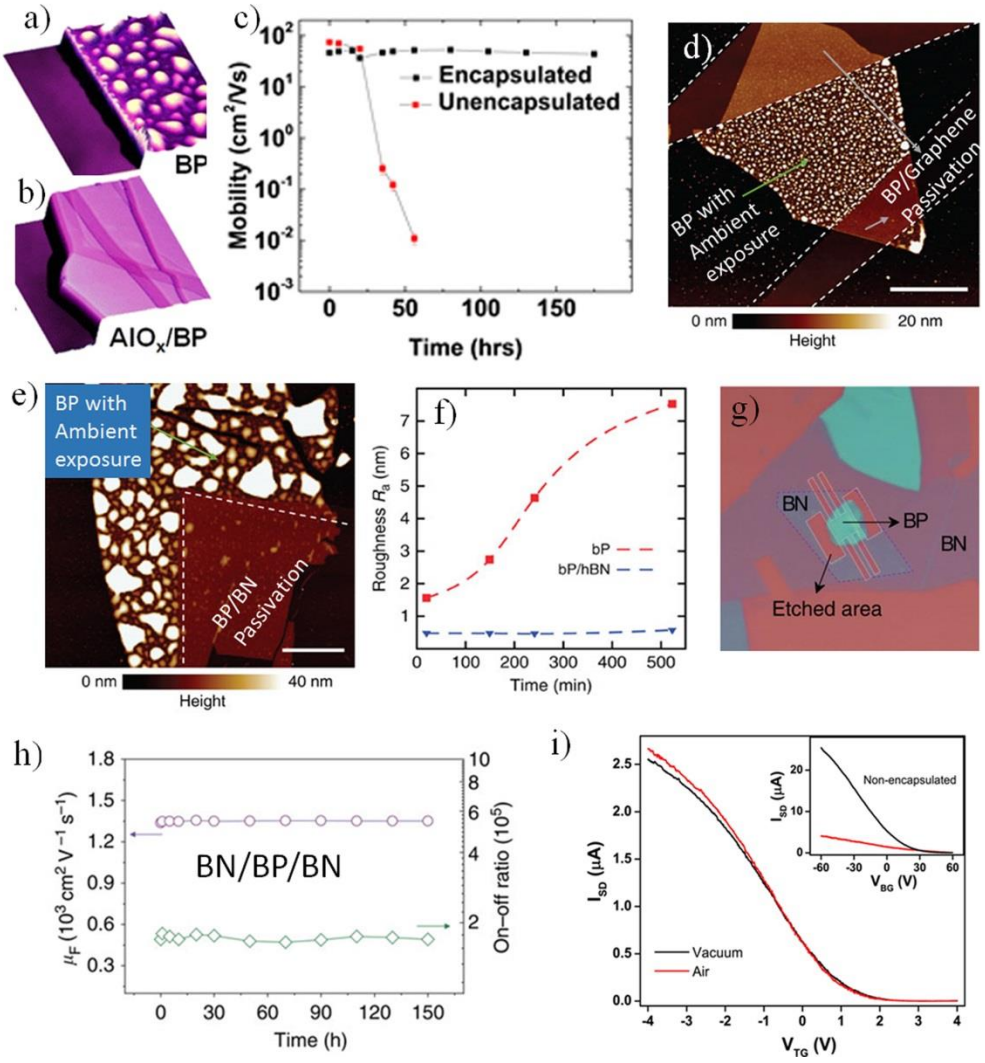

Figure 8. Passivation approaches for black phosphorus. a) and b) micrographic images of unencapsulated and AlO_x encapsulated BP. c) Hole mobility for encapsulated and unencapsulated Ti/Au contacted BP FETs (AlO_x, ref a and b) versus ambient exposure time. (a-c) Reproduced with permission.[190] Copyright 2014, American Chemical Society. d) AFM scans of a 5 nm thick BP crystal partly covered with graphene after 24 hours exposure to ambient conditions. e) AFM scan of a 10 nm thick BP crystal partly covered with h-BN after 5 days in ambient conditions. f) Average roughness (R_a) versus time for the passivated (blue triangles) and exposed (red squares) BP surface of the BP/h-BN sample. (d-f) Reproduced with permission.[44] Copyright 2015, Nature publishing group. g) Optical microscopic image of the BN–BP–BN heterostructure after O_2-plasma etching. h) Mobility and on–off ratio of BP as a function of ambient exposure time for the same BN-BP-BN structure. (g-h) Reproduced with permission.[41] Copyright 2015, Nature publishing group. i) Top gate voltage dependence of bias current from fully encapsulated BP device under vacuum (black line) and ambient conditions (red line) at fixed back gate (0 V) and source-drain (100 meV) biases. The inset shows the gate voltage dependence of a non-encapsulated device. Reproduced with permission [154] Copyright 2015, American chemical society.

Table 1. BP based FETs and their performances

Film thickness [nm]	Channel length [μm]	Gate insulator	Hole mobility [$cm^2 V^{-1} s^{-1}$]	On/off ratio	Ref.
10	1.6	SiO_2	984	10^5	18
5	1	SiO_2	286	10^4	9
5	1	SiO_2	205	$>10^5$	112
18.7	3	SiO_2	170	10^2	148
5	0.69	SiO_2	155	10^4	187
1.6	0.45	SiO_2	35	600	117
8.5	0.3	HfO_2	400	2×10^3	152
1.9	2	SiO_2 (back)/Al_2O_3 (top)	172	2.7×10^4	147
15 5	2.7	Polyimide (back)/Al_2O_3 (top)	310 180	10^3–10^4 10^4–10^5	157
~5	—	Ionic liquid	510	—	149
8	—	h-BN	1350	$>10^5$	41
10	—	h-BN	400	—	40

Table 2. Photo-responsivity and response time of different layered materials

Material	Measurement conditions	Responsivity [mA W^{-1}]	Response time [ms]	Spectral range	Ref.
>1L BP	V_{ds} = 0.2 V, V_g = 0 V, λ = 640 nm, P = 10 nW	~4.8	1	Visible–NIR	175
>1L BP	V_{ds} = 3V, V_g= -80 V, λ = 500 nm, P = 2-31 mW cm^{-2}	~9 x 10^7 ~1.82 x 10^3	2 x 10^5 1	UV Visible	46
>1L BP	V_{ds} = 50 mV, V_g = -30 V, λ = 633 nm, P = 60 nW V_{ds} = 50 mV, V_g = 0 V, λ = 633 nm, P = 60 nW	223 76	NA 100	Visible	186
11.5 nm BP 100 nm BP	V_{ds} = -4 V, V_g = -8 V, P = 1.91 mW V_{ds} = 2 V, P = 157 mW	135 657	NA	NIR	47
1L MoS_2	V_{ds} = 8 V, V_g = −70 V, λ = 561 nm, P = 150 pW	~880 × 10^3	600	Visible	167
>1L WS_2	V_{ds} = 30 V, V_g = N.A., λ = 458 nm, P = 2 mW	~21.4 × 10^{-3}	5.3	Visible	180
>1L In_2Se_3	V_{ds} = 5 V, V_g = 0 V, λ = 300 nm, P = 2.08 W m^{-2}	~395 × 10^3	18	UV–NIR	128
>1L GaS	V_{ds} = 2 V, V_g = 0 V, λ = 254 nm, P = 0.256 mW cm^{-2}	~4.2 × 10^3	30	UV–visible	182
>1L GaSe	V_{ds} = 5 V, V_g = 0 V, λ = 254 nm, P = 1 mW cm^{-2}	~2.8 × 10^3	300	UV–visible	181
>1L GaTe	V_{ds} = 5 V, V_g = 0 V, λ = 532 nm, P = 3 × 10^{-5} mW cm^{-2}	~10^7	6	Visible	170
>1L $MoSe_2$	V_{ds} = 20 V, V_g = 0 V, λ = 532 nm	~97.1 × 10^3	15	Visible	169

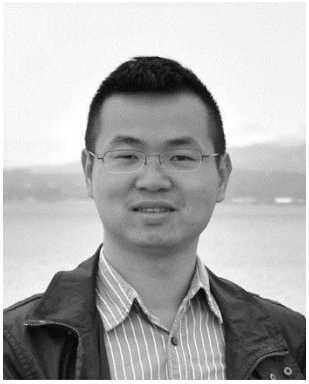

Dr. Zheng Liu was born in Hubei, China in 1983. He received his B.Sc. (2005) and Ph. D (2010) in Physics from National Center for Nanoscience and Technology (NCNST), China, under the guidance of Professor Lianfeng Sun. He is Nanyang Assistant Professor at Nanyang Technological University. His research focus on the growth, characterizations and performance of large-scale and high-quality novel low-dimensional crystals, including, hexagonal boron nitride, metal dichalcogenides and their hybridized architectures, as well as their applications on high-performance electronics, optical devices and energy conversion and storage.

Dr. Long obtained her PhD from Cambridge University, United Kingdom. Her PhD training is to study the mechanical property of the superlattice nitride thin coatings. Her current research interest is to develop functional coatings and focus on the optical, electrical and mechanical properties of nanocomposite, hybrid and ultra-thin coatings

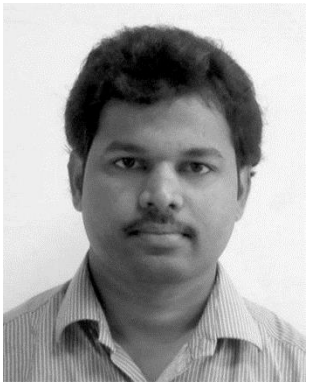

Dr. Varrla Eswaraiah was born in Kurnool, India in 1985. He received his M.Sc. degree in 2007 from Sri Venkateswara University, India. He earned Ph.D. in Physics on carbon nanotubes and graphene composites from IIT Madras, Chennai in 2012. During his first post-doctoral work at CRANN, Trinity College Dublin, Ireland, he worked on scalable approaches for 2D nanosheets. In 2015, he moved to Nanyang technological university, Singapore as a research fellow. His research focuses on developing energy efficient production and processing techniques for nanomaterials/nanocomposites for sensing, composites and electronics applications.

Black phosphorus (BP) exhibits extraordinary performance both in electronics and wide range optoelectronic devices due to its suitable bandgap. The unconventional anisotropy in BP arises from its puckered structure which makes it an anisotropic material at large magnitude. It also has potential applications in gas sensing at ultralow level detection towards various gases, energy storage devices and thermoelectric applications.

Black phosphorus, anisotropy, bandgap, electronics and optoelectronics

V. Eswaraiah, Q. S. Zeng, Y. Long,* Z. Liu*

Black Phosphorus Nanosheets: Synthesis, Characterization and Applications